

**POLITECNICO DI TORINO**

DEPARTMENT OF CONTROL AND COMPUTER ENGINEERING

Master degree course in Mechatronic Engineering

Master Degree Thesis

**Experimental investigation of mechanical abuses  
influences on local heat generation for an electrically  
cycled Lithium-ion battery**



Supervisor  
Prof.ssa Silvia Bodoardo

Company Supervisor  
Dott. Mag. Luigi Aiello

Candidate  
Gian Lorenzo Ninni  
ID Number: 266757

Academic Year 2019/2020



# ***Table of contents***

<i>1. Literature review on Lithium-ion batteries</i> .....	<i>1</i>
<i>1.1 Working principle of a lithium-ion cell</i> .....	<i>1</i>
<i>1.2 Battery internal components</i> .....	<i>3</i>
<i>1.3 Why separator is needed?</i> .....	<i>3</i>
<i>1.4 Battery Formats on market</i> .....	<i>7</i>
<i>1.5 Battery electrical behaviour</i> .....	<i>8</i>
<i>1.6 Capacitive effects and voltage relaxation</i> .....	<i>11</i>
<i>1.7 Aging phenomena in Lithium-ion batteries</i> .....	<i>14</i>
<i>1.7.1 Other factors affecting aging</i> .....	<i>16</i>
<i>1.8 Solid Electrolyte interface</i> .....	<i>17</i>
<i>1.9 What is lithium plating</i> .....	<i>18</i>
<i>1.9.1 How to detect lithium plating</i> .....	<i>21</i>
<i>2. Abuse case under analysis</i> .....	<i>23</i>
<i>2.1 Mechanism and degree of failure</i> .....	<i>23</i>
<i>2.2 Thermal runaway mechanism</i> .....	<i>24</i>
<i>2.3 Thermal abuse</i> .....	<i>26</i>
<i>2.4 Electrical abuse</i> .....	<i>27</i>
<i>2.5 Mechanical abuse</i> .....	<i>28</i>
<i>2.6 Mechanical abuse test</i> .....	<i>29</i>
<i>2.7 Internal behaviour during mechanical abuse</i> .....	<i>31</i>
<i>2.8 Separator mechanical properties</i> .....	<i>33</i>
<i>3. Test design</i> .....	<i>35</i>

3.1 Purpose of the tests .....	35
3.2 Battery under test.....	35
3.3 Structure of tests.....	37
3.5 Penetrator design.....	43
3.6 Temperature sensors .....	52
3.7 Pliers and plates design .....	55
3.8 Mounting sequence .....	58
4. Experiment results.....	61
4.1 Results of the first tested battery .....	61
4.1.1 Electrical cycling between 20% and 30% of SOC.....	62
4.1.2 Voltage relaxation after reaching SOC of 90%.....	65
4.2 Results of the second tested battery .....	68
4.3 Results of the third tested battery.....	70
5. Conclusions .....	72
5.1 Post-processing of data.....	72

## *List of Figures*

Figure 1 - Lithium in stable configuration and ionized configuration.....	1
Figure 2 – Example of one of the simplest electrochemical cells .....	2
Figure 3 - Example of a jellyroll composition of a cylindrical battery.....	4
Figure 4 - Side view of PP/PE/PE tri-layer.....	5
Figure 5 - Equivalent circuit for resistance of a separator .....	6
Figure 6 - The different battery formats available on market.....	7
Figure 7 - Internal layer structure of pouch cell .....	8
Figure 8 - Discharging curves at different C-rates .....	9
Figure 9 - Hybrid Pulse Power Characterization (HPPC) test profile example <sup>25</sup>	10
Figure 10 - Internal resistance measurement based on the current charge/discharge pulses at both current switch on and switch off.....	11
Figure 11 - Double layer region under conditions where anions are specifically absorbed <sup>26</sup> .....	12
Figure 12 - Voltage response of a battery after charge.....	13
Figure 13 - Overview on aging phenomena.....	15
Figure 14 - Sketch of SEI film.....	17
Figure 15 - Increase in temperature due to SEI film.....	18
Figure 16 - Lithium ions have some difficulty to intercalate into the anode.....	19
Figure 17 - Schematic of (a) the intercalation and plating currents during charging to higher states of charge and (b) the re-intercalation of deposited lithium during rest <sup>7</sup> .....	19
Figure 18 - Dendrite growth between electrode and electrolyte (from Web)....	20
Figure 19 - Difference in voltage relaxation with and without lithium plating..	22
Figure 20 - Most common causes of thermal runaway <sup>15</sup> .....	23
Figure 21 - Explosion of battery due to abusive test (via Web) .....	24
Figure 22 - Qualitative interpretation of the chain reactions during thermal runaway <sup>15</sup> .....	25
Figure 23 - Different stages of temperature response <sup>9</sup> .....	27

Figure 24 – Example of denting on a pouch battery.....	29
Figure 25 – Example of indentation test.....	30
Figure 26 – Example of pinch test.....	30
Figure 27 - Cross-section view on nail penetration .....	31
Figure 28 - Internal deformation of Li-ion cells after pinch tests.....	32
Figure 29 - Cross section image of Li-ion cell pinched.....	33
Figure 30 - SEM characterization of separator membranes after compressive stress testing.....	34
Figure 31 - Example of battery under test .....	36
Figure 32 - Microscopic view of internal layers arrangement of the battery .....	36
Figure 33 - Microscopic view of the separator .....	37
Figure 34 - Scheme of Tests .....	38
Figure 35 - CCCV charging method.....	40
Figure 36 - Exploded view of the assembly .....	42
Figure 37 - Five punch heads used in indentation tests <sup>18</sup> .....	43
Figure 38 - Force, OCV and local temperature increase versus intrusion curves of a pouch cell under flat-end cylinder indentation <sup>18</sup> .....	44
Figure 39 - Force, OCV and local temperature increase versus intrusion curves of a pouch cell under hemispherical head indentation <sup>18</sup> .....	45
Figure 40 - Force, OCV and local temperature increase versus intrusion curves of a pouch cell under conical head indentation <sup>18</sup> .....	45
Figure 41 - Relative intrusion at inflection point, peak force point, OCV drop and temperature increase in the pouch cell and prismatic cell under different loadings <sup>18</sup> .....	46
Figure 42 -. Load-displacement curves for small, medium and large hemispherical impactor <sup>19</sup> .....	46
Figure 43 - Drop voltage for small, medium and large hemispherical impactor <sup>19</sup> .....	47
Figure 44 - Peak load (left) and deformation depth (right) at short circuit versus	

the diameter of the punch <sup>19</sup> .....	47
Figure 45 - Load displacement curves of a pouch cell under hemispherical head indentation for nine different position (top) and Cell voltage displacement curve (bottom) .....	48
Figure 46 - Different contact points utilized during a previous test in VSI.....	49
Figure 47 - First prototype of the impactor.....	49
Figure 48 - Final prototype of the impactor.....	50
Figure 49 - Cross section of the impactor with internal channel exposed.....	51
Figure 50 - Explanatory image of the available point of impact .....	52
Figure 51 - Graph containing the changes of resistance with temperature for a platinum resistance thermometer and a thermistor <sup>21</sup> .....	53
Figure 52 - PT1000 sensor.....	54
Figure 53 - Explanatory image of temperature sensors' location.....	54
Figure 54 - Solidworks sketch of Aluminium plier .....	55
Figure 55 - Superior piece of Aluminium plier .....	55
Figure 56 - Real Aluminium pliers under use.....	56
Figure 57 - Bottom view of inferior Pertinax plate .....	57
Figure 58 - Cavalieri's axonometry of inferior plate of Pertinax.....	57
Figure 59 - Top view of the superior Pertinax plate used to allow the transit of the impactor .....	58
Figure 60 - Full metal plate and Pertinax plate on wood block.....	58
Figure 61 - Addition of superior Pertinax plate.....	59
Figure 62 - Full sandwich for the tests .....	59
Figure 63 - Full setup for the test.....	60
Figure 64 - Comparison between pristine battery and impacted battery in cycling between 20% and 30% of SOC at 1C-rate.....	62
Figure 65 - Closer look to a single cycle between 20% and 30% of State of Charge at 1C-rate .....	63
Figure 66 - Closer look to a single cycle between 20% and 30% of State of	

Charge at 2C-rate .....	64
Figure 67 - Closer look to a single cycle between 20% and 30% of State of Charge at 2C-rate .....	64
Charge at 3C-rate .....	65
Figure 68 - Overview of charging until 90% SOC at 1C-rate followed by voltage relaxation .....	66
Figure 69 - Closer look to voltage relaxation executed at 1C-rate .....	66
Figure 70 - Closer look to voltage relaxation executed at 2C-rate .....	67
Figure 71 - Closer look to voltage relaxation executed at 3C-rate .....	67
Figure 72 - Temperature data of 0%-90% 1C of third battery.....	71
Figure 73 - Reference curves for comparisons .....	72
Figure 74 - Example of the type of comparison between the 1C pristine curve and 2C Pristine curve.....	73
Figure 75 - Subtraction of 2C pristine curve with 1C pristine curve.....	74
Figure 76 - Plot of all the subtraction curves obtained.....	74
Figure 77 - Integrated curve of the subtraction.....	75
Figure 78 - Pristine versus Impacted comparison regarding Lithium plating ....	76

## ***List of tables***

<i>Table 1 - Table of executed tests</i> .....	39
Table 2 - Example of steps of charge/discharge programmed on battery tester for electrical cycling 20%/30% .....	40
Table 3 - Example of steps of charge/discharge programmed on battery tester for electrical cycling 0%/90% .....	41
Table 4 - Results of the first battery tested .....	61
Table 5 - Results of the second battery tested .....	68
Table 6 - Results of the first battery tested .....	70
Table 7 - Results of the quantitative measures of Lithium plating.....	76



## *Abstract*

The effort to save the modern society from energy crisis and the even more alarming environmental pollution has been made for years with challenges and hopes mutually emerging. The change of energy storage and propulsion system is driving a revolution in the automotive field to develop new electrified power-train system and storage system. In this context, Lithium-ion battery made its way along different storage systems because of its significant advantages such as high energy density, low self-discharge rate and high operative voltage. Now, with continuous improvement in lithium ion batteries energy density, enhancing their safety is becoming increasingly urgent for the electric vehicle development.

Therefore, abstracting the daily usage of a battery pack, the cells undergo under several stress like temperature variation and different charging conditions and, during crash, mechanical stress could be encountered. Over the years, many tests have been developed to simulate the different stress and damage encountered during crash (ex. nail penetration). Lot of effort has been put into studying abusive and disruptive damage but only few takes into consideration non-disruptive damages. This work wants to develop a series of non-disruptive test in order to find differences between a fresh battery and a mechanically loaded one regarding heat generation, voltage variations during electrical cycling and appreciable changing in voltage plateau.

The battery under analysis is a laminate pouch-type cell, composed by Graphite as anode material and a spinel of NMC and LMO as Cathode material, with a rated capacity of 41Ah and a nominal voltage of 3.7V. The wanted impact was developed with a pressure applied on a custom plastic impactor. During all the tests voltage and temperature of the battery were registered in order to perpetrate the objectives set and understanding the causes of them.



## *Introduction*

Transport is one of the main causes of CO<sub>2</sub> emission, the most important greenhouse gas (GHG) and if we, as human species, will not be able to drastically reduce this malicious production the consequences could be bad if not catastrophic. Even in those regions where CO<sub>2</sub> emissions from other sectors are generally falling, those from transport have continued to increase. In Europe, for example, between 1990 and 2012, total GHG emission decreased by almost 18% but those from transport increased by about 14%<sup>13</sup>. Reducing emissions in transport is costlier than in other sectors, such as electricity sector and the reason for this is that transport still heavily relies on fossil fuels. Until the cost of alternative vehicle falls enough to be interesting for most people, taxes and subsidies from the governments are needed. In addition to subsidizing clean technologies to make them more attractive, government support for R&D is also needed around the globe. During the years, multiple progress has been made to make electric vehicle more appealing; for example, Tesla bet on high performance electric vehicles in order to try to erase the impression settled over years among the people that electric vehicles are slow and inefficient.

Nevertheless, to really conquer the market the crucial issues to deal with are range and recharge time. For what concerns the problem of little autonomy, this can be obtained from an increasing in aerodynamic efficiency of the vehicle or, more consistently, with higher energy density batteries. Instead, for what regards reduction of charging times, batteries that can receive a high-power input are needed. Both those conditions bring a question to mind: an increase in energy density and charging rate represent a further hazard in terms of safety?

The answer is, of course, yes. Nevertheless, this only means that we need to set the bar even higher in terms of security. The raise in selling needs to go hand in hand with the improvement in security matter and that is where this work stands. When the electric vehicles will represent a preponderant percentage in our streets, crashes will be a daily occurrence and we need by that time a precise protocol to estimate damages of the batteries. Just during the daily usage, Lithium-ion batteries undergoes under several abuses such as overcharge, elevated or really low ambient temperature, vibrations. In addition, we need to pay attention to possible damage resulting from collisions and their consequences. The totality of accident happening daily are not always severe, so we need to understand how also a non-severe damage affect the behavior of batteries. Several studies have been made regarding severe damage but only few takes into consideration moderate abuse. This work takes part to the “Safe Battery” research project, financed by seven industrial partners (Daimler, Bosch, Audi, Porsche...) with the objective to

give a research contribution to the understanding of the hazard conditions of Li-ion batteries under various mechanical loading conditions. In particular, in case of “non-critical” mechanical load, acceleration or permanent deformation, it is of interest the understanding of the heat generation distribution of the Li-ion battery under electrical loads. Main objective of this research is the complete understanding of this phenomenon, a mathematical formulation of the problem and the causes of it.

First of all, we need to define in a precise way a moderate damage: a non-severe abuse happens when, for example, during a penetration with a tip we impact several layers of the battery but not causing internal hard short circuit, only the soft short circuit are allowed. The first analysis before tests was, so, understand how to exactly generate a mechanical abuse on the battery without fall back into a disruptive test but staying borderline. Before thinking about the real tests design, our research question was focused principally on three phenomena: local heat generation variation, voltage variation during cycling and changing in Lithium plating. For the first two point, tests were conducted to emphasize them and how we did that will be described through the chapters. The last one of these phenomena comes naturally with the aging of the battery, leading to inefficiency; during these tests will be seen if changing caused by mechanical load can be possible.

The following work has been organized as follow: the first chapter summarize the working principle of a Lithium-Ion battery and the main phenomena that characterize the aging of it. The main focus was put on the Lithium plating and SEI formation. In the second chapter, the concept of abuse and how to reach the type of abuse required was documented. In the third chapter, an overview on the tests was provided and particular attention was put on the description, step by step, of the design of all the tools and the reasons behind the need of them. In the fourth chapter, all the data coming from the tests are plotted with a brief comment on the phenomena obtained. Finally, in the fifth and last chapter, the results are shown and all the reasons that had led to those are explained.

# CHAPTER 1

## *1. Literature review on Lithium-ion batteries*

### *1.1 Working principle of a lithium-ion cell*

Lithium ions batteries are widely used nowadays to store energy in electrochemical form and then deliver that later under electrical charge to power a load circuit. Every Li-ions battery works on the concept of electrochemical potential associated with metals. Electrochemical potential is the tendency of a metal to lose electrons and it is measured in Voltage (V) so, the higher Voltage is, the higher is the propensity to give up an electron on the last energy level. Lithium, having only one electron in his outer shell, is a high reactive metal and has a 3.04 V of Electrochemical potential, meaning that has a high tendency to lose that electron. However, Lithium in a metal oxide is much more stable, so, if we can provide two different paths, one for electrons and one for lithium ion flow, between lithium and the metal oxide, the lithium ion will be able to intercalate into the metal oxide.

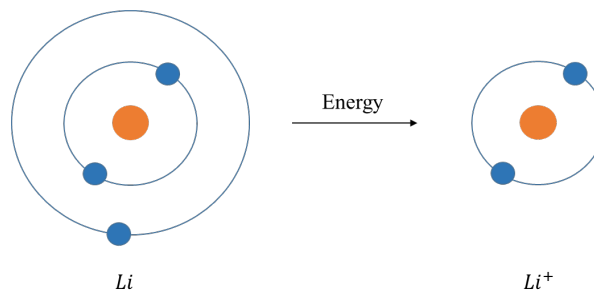


*Figure 1 - Lithium in stable configuration and ionized configuration*

In an electrochemical cell, the anode is where oxidation takes place and the cathode is where reduction takes place. As the reaction proceeds in a galvanic cell, the electrons released at the anode travel through the external circuit. They re-enter the cell at the cathode, where they bring about reduction<sup>1</sup>. The main purpose of the electrochemical reactions is to sustain a steady state current flow into the galvanic circuit and in particular at the electrodes/electrolyte interface. Differently from a common redox chemical reaction, in Li-ion batteries an “insertion-electrode reaction” happens lithium does not react directly with

the electrode materials. Instead it is either absorbed from the electrolyte and inserted into the structure of the electrode material (process known as intercalation) or expelled from the electrode material into the electrolyte (process known as de-intercalation), depending on the direction of the current flow.

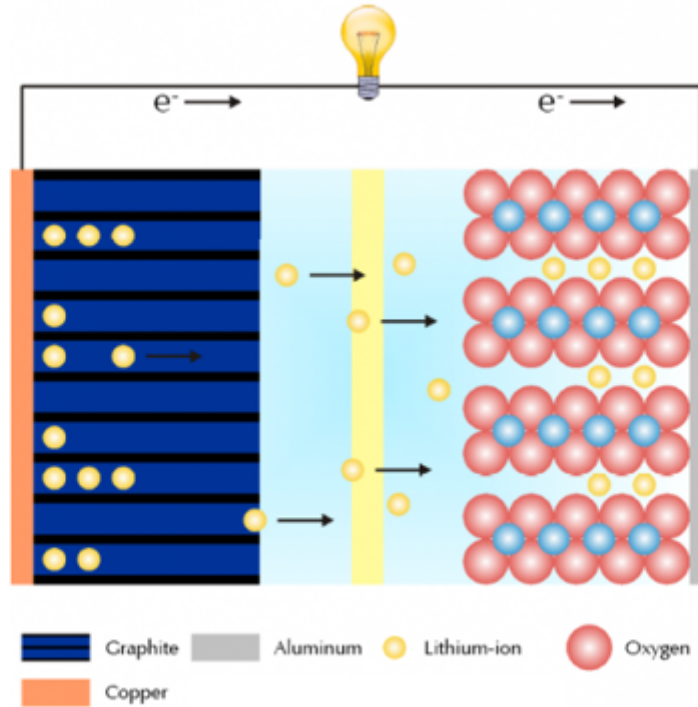
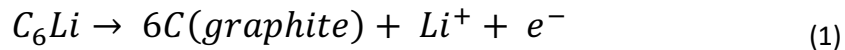
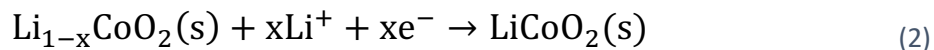


Figure 2 – Example of one of the simplest electrochemical cells

During discharge, lithium is oxidized from Li to Li<sup>+</sup> (0 to +1 oxidation state) in the lithium-graphite anode through the following reaction:



These lithium ions migrate through the electrolyte medium to the cathode, where they are incorporated into lithium cobalt oxide through the following reaction, which reduces cobalt from a +4 to a +3 oxidation state as in (2):



These reactions can be run in reverse to recharge the cell. In this case the lithium ions leave the lithium cobalt oxide cathode and migrate back to the anode, where they are reduced back to neutral lithium and reincorporated into the graphite network.

## ***1.2 Battery internal components***

The basic arrangement, independently from the chemistry and the shape that the battery has, is always the same. Here a schematic description:

- Electrodes: must have two key properties: first, they must have open-crystal structures, pervaded with empty ‘corridors’ that are large enough for lithium to move through freely. Second, the electrodes must also be able to deliver or accept compensating electrons to/from the external circuit at the same time<sup>2</sup>.
- Negative Electrode (anode): often made of some form of graphite ( $C_6$ ). Graphite comprises multiple graphene layers and lithium intercalates between these layers.
- Positive Electrode (cathode): here the choice is not obligatory as the anode; a good choice can be the lithium cobalt oxide ( $Li_xCoO_2$ ) which behave somewhat like graphene in graphite and that is the reason why the cathode made of this material is often called layered cathode. The choice could also fall on lithium manganese oxide ( $Li_xMn_2O_4$ , or LMO) as an alternate intercalation compound.
- Electrolyte: is the media that conducts ions between electrodes. It comprises either a salt, an acid, or a base that is dissolved in a solvent. Water cannot be used since lithium reacts violently with it, so the electrolyte has to be made composed of non-aqueous organic solvents plus a lithium salt and acts purely as ionic conducting medium.
- Separator: porous membrane that allows through unimpeded but small enough that the electrodes particles do not make contact through the holes. It is also an electronic insulator.

## ***1.3 Why separator is needed?***

When a simple galvanic cell is taken into consideration, having only one anode and one cathode, the risk of short circuit occurrence is practically impossible to happen. Nevertheless, with the high expectations from the market on the performance and safety of

Lithium-ion batteries, dutiful implementations are needed. If anode and cathode are in charge of enhance the performance, components like electrolyte and separator are in charge of safety because put together a lot of layers of electrodes require an efficient electronic insulation as shown in Figure 3.

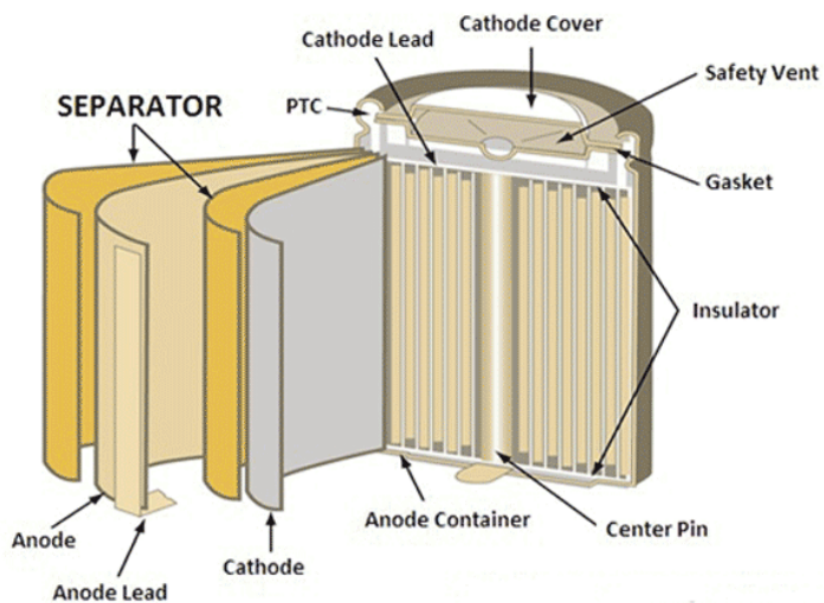


Figure 3 - Example of a jellyroll composition of a cylindrical battery

A battery separator is a polymeric membrane placed between the positively charged anode and negatively charged cathode to prevent an electrical short circuit. Although ions pass freely between the electrodes, the separator is an isolator with no electrical conductivity. The small amount of current that may pass through the separator is self-discharge and this is present in all batteries to varying degrees<sup>23</sup>. Early in the days, separator was made of rubber, glass fibre mat and polyethylene plastic. Wood was the original choice, but it reacts and deteriorates with the electrolyte. The actually commercially available Lithium ion cells use polyolefin as separator. This material has excellent mechanical properties and good chemical stability. A polyolefin is a class of polymer that is produced from olefin by polymerizing olefin ethylene. Ethylene comes from a petrochemical source; polyolefin is made from polyethylene, polypropylene or laminates of both materials<sup>23</sup>. Nowadays, separator has a tri-layered structure, as shown in Figure 4, that allows an enhanced fuse protection on thermal abuses.

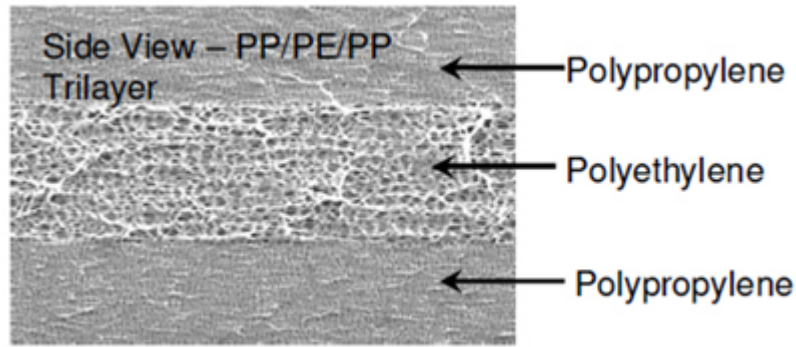


Figure 4 - Side view of PP/PE/PE tri-layer

The tri-layer structure consists of polyethylene (PE) in the middle that is sandwiched by outer polypropylene (PP). This choice is due to the two different melting points of these material: while the inner PE layer shuts down at 130° by closing the pores, the outer PP layers stay solid and do not melt until reaching 155°C.

The Li-ion separator must be permeable and the recommended porosity is 30% to 50% in order to holds enough liquid electrolyte and enables the pores to close when the cell overheat<sup>23</sup>. Since the separator is filled with electrolyte, understanding the ionic resistivity of the electrolyte is the key to understand the resistivity of the separator itself. The quantity of electrolyte in the separator, however, is driven by concept as porosity and tortuosity. The porosity  $\epsilon$  is a well-defined property of a porous medium, which can be determined easily. On the contrary, the effective tortuosity  $\tau$  of separator is difficult to calculate in a precise way and, to complicate even more the calculation, a lot of different definition of tortuosity are used. The effect of a porous microstructure on the macroscopic conservation law can be described by the MacMullin number  $N_M$ :

$$N_M = \frac{k}{k_{eff}} \quad (3)$$

Which relates the ionic conductivity  $k$  of the electrolyte solution to the effective ionic conductivity  $k_{eff}$  of a porous separator<sup>24</sup>. In contrast, it is possible to use a microscopic approach to a model a porous microstructure. In this case, the tortuosity can be seen as a measure of the elongation of the transport path due to porous structure with respect to a

straight-line  $d$  as shown in the Equation 4:

$$\tau_{path} = \frac{d_{path}}{d} \quad (4)$$

In addition, tortuosity can also take into consideration the shortest connection between two points, defining the geometrical tortuosity  $\tau_{geo}$ . Therefore, a constriction factor  $\beta$  can be introduced to consider also the non-constant cross-sectional area using the Equation 5:

$$N_M = \frac{\tau_{geo}}{\varepsilon\beta} \quad (5)$$

Charge transport in porous particle network or structure as lithium ion battery electrodes or separators is determined by the ionic resistance  $R_{ion}$  inside the electrolyte phase. If the ionic resistance  $R_{ion}$ , porosity and thickness can be determined, tortuosity can be calculated by rearranging Ohm's law<sup>24</sup>:

$$N_M = \frac{\tau}{\varepsilon} = \frac{R_{ion} * A * k}{d} \quad (6)$$

Impedance measurements of electrolyte-filled separators can be described by an equivalent circuit consisting of a serial connection of two constant-phase Elements (CPEs) and an ionic resistance, where the two CPEs can be merged into one CPE as shown in Figure 5:

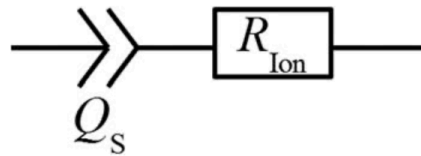


Figure 5 - Equivalent circuit for resistance of a separator

The impedance of the equivalent circuit in Figure 5 is given by:

$$Z_{Sep} = R_{Ion} + \frac{1}{Q_s(i\omega)^\gamma} \quad (7)$$

Which allows for a simple determination of the ionic resistance  $R_{Ion}$  inside the porous separator by means of a high frequency extrapolation ( $\omega \rightarrow \infty$ ) in the corresponding Nyquist plot.

### ***1.4 Battery Formats on market***

A first distinction needs to be done between cells and batteries; cells are the smallest individual electrochemical unit and deliver a voltage that depends on the combination of chemicals and compounds chosen to make the cell itself. Single use cells are called primary cells and rechargeable cells are called secondary cells. Batteries, instead, are made up from groups of cells. The elements that make up a battery cell can be arranged in different ways, depending on the chosen form factor. Mainly, it is possible to distinguish three types of cells:

- Cylindrical cells
- Prismatic cells
- Pouch cells

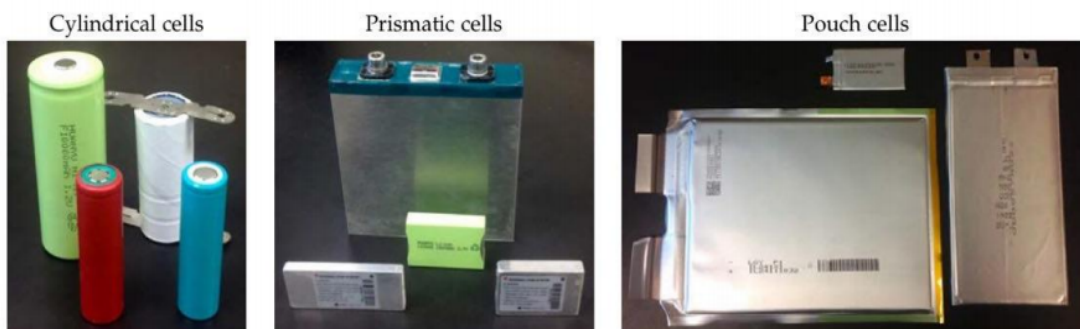


*Figure 6 - The different battery formats available on market*

In each case, the cells contain one or more negative and positive electrodes connected in parallel inside the cell, forming a single logical negative and positive electrode. Cylindrical cells are most common, and we are used to deals daily with them also when batteries were

not used in automotive applications. Prismatic and pouch cell are finding heavy use for high-capacity battery applications to optimize the use of volume in high-capacity battery packs, since the more rectangular shapes pack together better.

Pouch cells, the ones with whom we work, are assembled by stamping electrode plates out of the reels of electrode-coated foil and stacking alternately negative and positive electrode plates, interrupted by the separator material. Then, in order to obtain a single logic electrode, all the electrode tabs are welded in parallel.

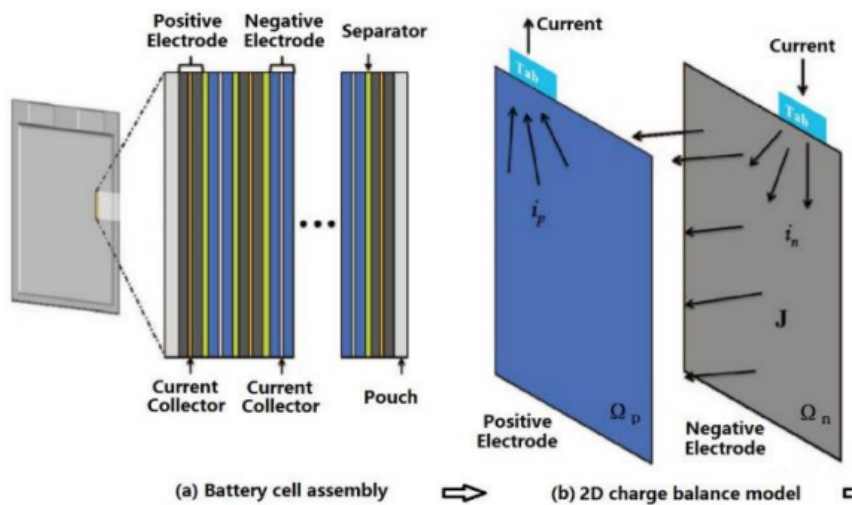


Figure 7 - Internal layer structure of pouch cell

### 1.5 Battery electrical behaviour

The cell nominal charge capacity defines the quantity in charge, in ampere-hours (Ah) or milliampere-hours (mAh), that a cell is rated to hold. Instead, the cell nominal energy capacity is the quantity of electrical energy in watt hours (Wh) or kilowatt hours (kWh) that the cell is rated to hold and is computed as the cell's nominal voltage multiplied by its nominal charge capacity. However, when later the term capacity will be said, it will refer to charge capacity and not to energy capacity.

The rate capability of a battery can be defined as the rate at which the cell is being charged. The C-rate is a relative measure of cell current. It is the constant-current charge or discharge rate that the cell can sustain for 1 hour or, more simply, the nominal ampere hour rating of the cell multiplied by  $1h^{-1}$ . For example, when a 40 Ah battery is loaded with a certain current - as example 20A - then its charging rate is considered as the actual current

normalized with respect to the nominal current. The rate capability and capacity of Li-ion batteries are dependent on their design and varies considerably between different manufactures.

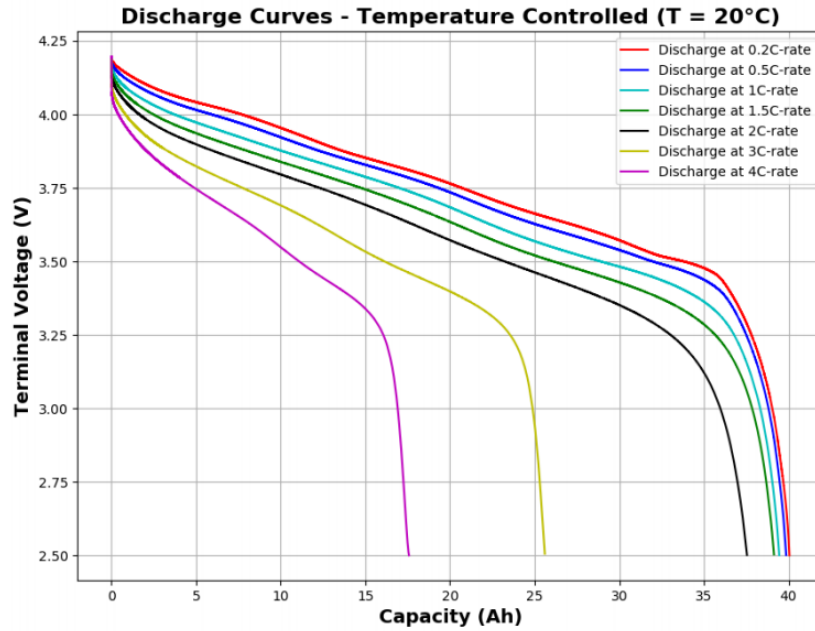


Figure 8 - Discharging curves at different C-rates

Note that the relationship between Terminal Voltage and Capacity at different C-rate is not strictly linear; this because of the internal resistance of the battery cell and also for the incomplete utilization of the active materials when the cell is exercised at high rates. This non-linear relationship can also be seen between C-rate and discharge rate.

A lot of work was done by researchers around the world to develop a wide variety of techniques able to model the battery. One of the most important tests to identify the dynamic properties of the battery is called Hybrid Power Pulse Characterization (HPPC) test; this test run on the principle that a current pulse will cause a corresponding voltage pulse according to the simple equation:

$$V_{pulse} = I_{pulse} * R \quad (8)$$

The battery is charged and discharged under a controlled condition and the terminal voltage, current and temperature are monitored<sup>25</sup>. A HPPC test profile is shown in Figure 9:

## HPPC Profile

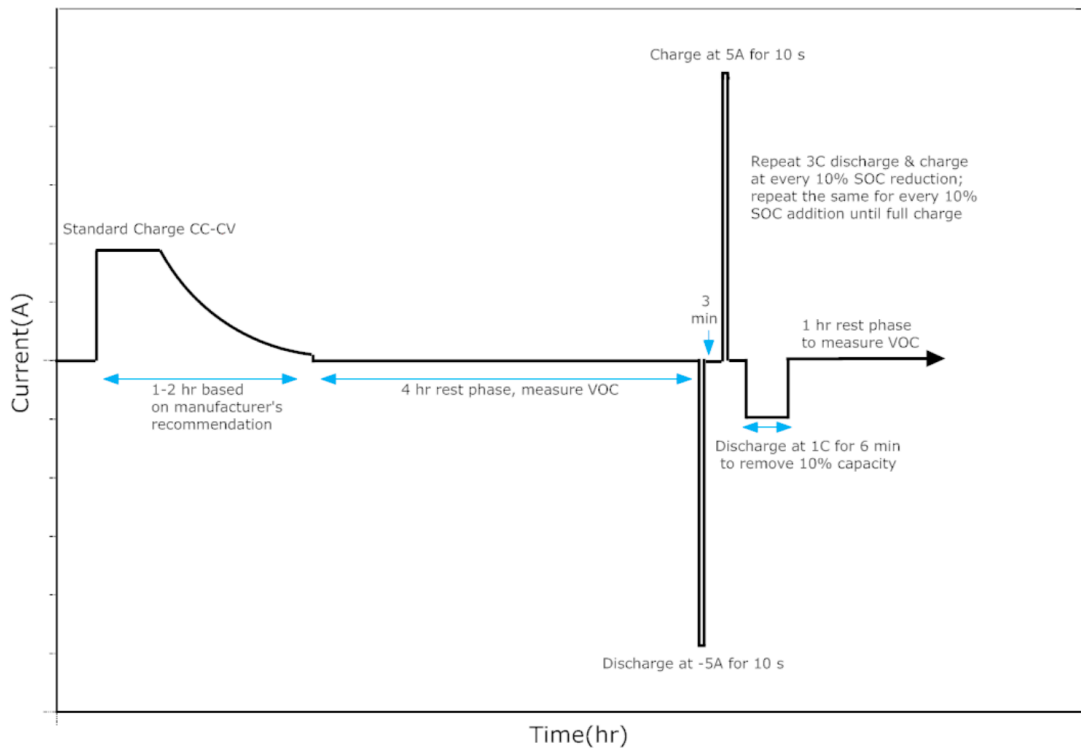


Figure 9 - Hybrid Pulse Power Characterization (HPPC) test profile example<sup>25</sup>

Ideally the power pulse characterization should be done at a high C-rate charge/discharge rate but in the example above for some limitation of the battery cyclers, the maximum charging and discharging was done at 5A. The cell rests for 3 minutes and then discharged for 6 minutes at 1 C rate to achieve a 10% decrease in SOC. Afterwards the cell rests for 1 hour to reach equilibrium before the next HPPC test profile begins. The partial discharge-HPPC- rest phase cycle is repeated at decrements of 10% of SOC till the cell reaches 10% SOC. The process is repeated in the charging direction as well<sup>25</sup>. The cell shows an increased voltage during charge and a decreased voltage during discharge. The difference occurs due to the polarization voltage which can be attributed to two mechanisms. One mechanism is the overpotential at the electrodes caused by the electro chemical reactions and concentration deviations due to the transport phenomena. The other mechanism is an ohmic voltage drop across the current collectors and electrolyte when there is a current flow. The result of the test is a characterization of the internal resistance at difference State of Charge (SOC) and, obviously, the more accurate the characterization is required, more steps would be needed (an example is given in Figure 10). Besides the HPPC test, other methods and techniques are also investigated to calculate the internal resistance of the cell. The most

common method of measuring the internal resistance of the cell is called ‘‘Current step pulse technique’’. The difference in respect to the HPPC test is the characterization of the resistance based on the immediate jump in the terminal cell voltage with no care about the possible voltage relaxation.

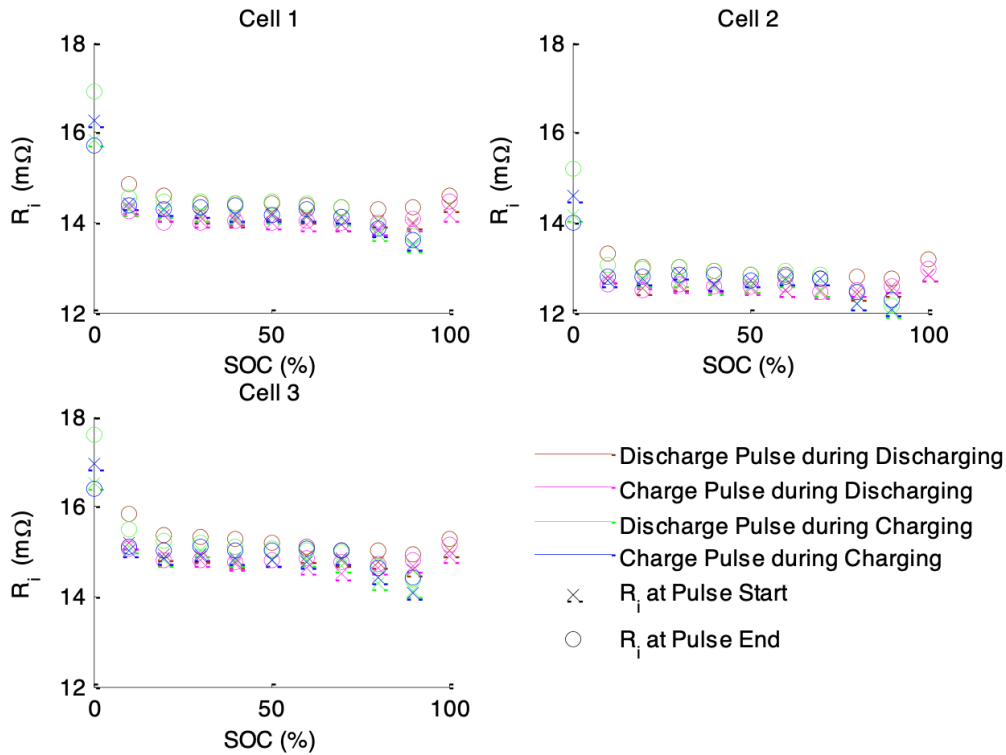


Figure 10 - Internal resistance measurement based on the current charge/discharge pulses at both current switch on and switch off

### 1.6 Capacitive effects and voltage relaxation

The electrical double layer (EDL) is a structure that appears whenever two conducting phases meet at interphase, in the specific case of Lithium-ion batteries at the interphase between the electrode (solid) and the electrolyte (liquid). When we deal with charged surface (electrode) there must be a balancing counter charge and this counter charge will occur in the liquid. However, the charges will not be uniformly distributed through the liquid phase but will be concentrated near the charged surface. The structure is made up of several layers: the closest to the electrode, the inner layer, contains solvent molecules and sometimes other species (ions or molecules) that are said to be specifically absorbed<sup>26</sup>. The

locus of electrical centres of the specifically adsorbed ions is called the “inner Helmholtz plane” which is at a distance  $x_1$ . Solvated ions can approach the metal only to a distance  $x_2$ ; the locus of centres of these nearest solvated ions is called the “outer Helmholtz plane”. These ions are said to be non-specifically adsorbed and their interaction with the charged metal involves only long-range electrostatic forces.

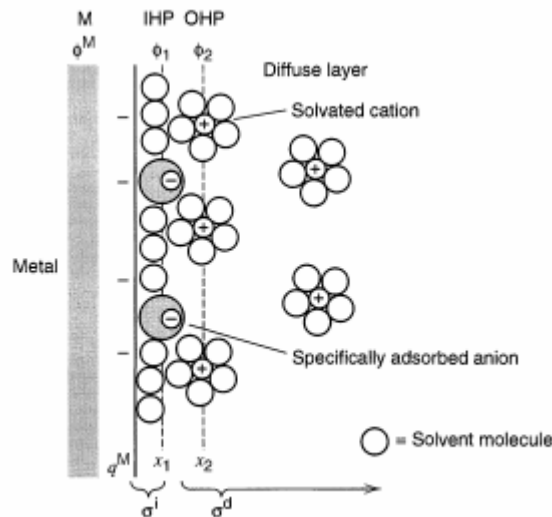
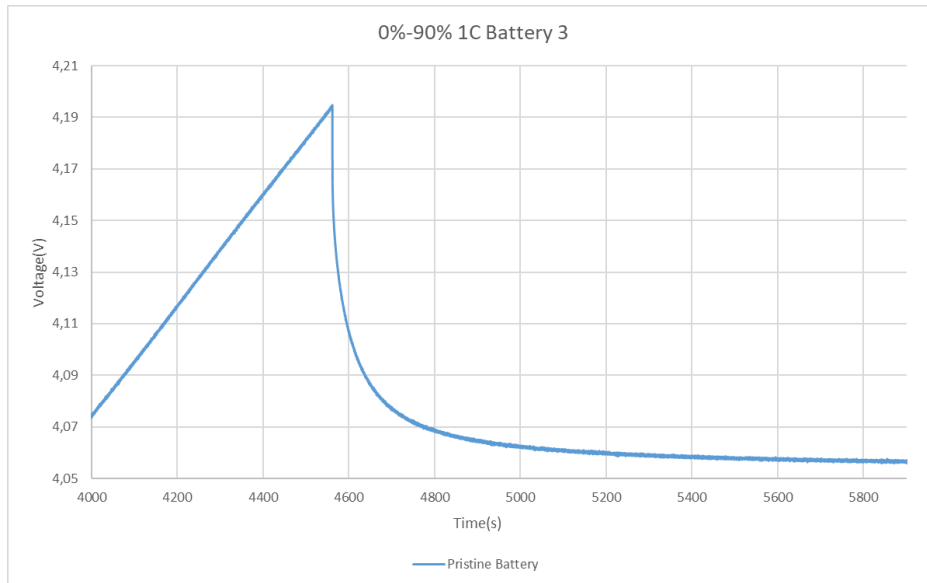


Figure 11 - Double layer region under conditions where anions are specifically adsorbed<sup>26</sup>

A very high capacitance can be associated with the electrical double layer because its existence can affect the rates of electrode processes. If a species that is not specifically adsorbed is taken into consideration, the approach with the electrode will happen only at the OHP.

After being charged or discharged, the battery voltage does not stay still but, on the contrary, keeps evolving towards a finite value, even if no current is exchanged with the battery. This phenomenon is called *voltage relaxation* and can last hours or even days. This behaviour is explained because phenomena inside the battery, such as polarization and mass transfer, have very slow dynamics and occur during hours of relaxation phase, causing voltage variations<sup>17</sup>.



*Figure 12 - Voltage response of a battery after charge*

For example, Figure 12 shows the typical voltage response of a battery following a charge cycle. The relaxation corresponds to the phase after the period of charge, during which there is no current applied and the battery voltage tends towards a steady state. The voltage measured after this temporary phenomenon can be considered as the Open Circuit Voltage (OCV) value at this SoC (in this case 90%). Relaxation time has, also, a significant impact on the measured voltage, which is considered to be the OCV at the end of relaxation, so when the relaxation time increases, the value of relaxation voltage measured in discharge increases and the one in charge decreases. The longer the relaxation time, the more the measurement of the battery voltage will be close to the real OCV, in fact it was stated that it may take over 24 hours before the battery voltage stabilizes. If the voltage variation during the relaxation is not taken into account in OCV estimation, error will be introduced into the estimation of SoC from the voltage.

## ***1.7 Aging phenomena in Lithium-ion batteries***

Aging is an unwanted, but at the same time inevitable, phenomenon that deteriorates batteries performance; it is generally irreversible and eventually results in cell failure. It is necessary to study battery aging mechanisms for the establishment of a connection between the degradation of battery external characteristics (terminal voltage or temperature) and internal side reactions, in order to be able to provide accurate predictions of internal behaviour of the battery. The entire life of a battery includes cycle life and calendar life. In the cycle process, there are inevitable side reactions (also called aging reactions) other than the main reactions inside a battery, which lead to a decrease in battery power and capacity and an increase in internal resistance as the number of cycles increases. It is commonly accepted that 80% of the rated capacity marks the end of battery life.

The following figure shows internal physical and chemical reactions and external characteristics influenced by aging from perspectives of anode, cathode and other parts of the battery such as inactive material<sup>4</sup>.

As can be seen, most of the internal aging reactions happen at the anode and cathode. Even if a large number of phenomena happens also in the inactive materials, it is useful to consider only those phenomena that really impact on battery performance. It has been demonstrated<sup>5</sup> that phenomena like Solid Electrolyte Interface (SEI) formation and Lithium plating are capable of produce 75% of the total capacity loss get during the life cycle.

Any of the previous phenomena could causes, after enough charge/discharge cycles, to one or more of the following undesirable effects:

- Increased internal impedance: the resistance of the cell increases and, as result, the power that the cell is capable of delivering is diminished and this leads to power fade.
- Reduced capacity: the decline of capacity over time is known as capacity fade and normally is irreversible.
- Increased self-discharge: the self-discharge rate of the cell tends to increase over time due to electrode swelling, dendritic growth or local overheating.

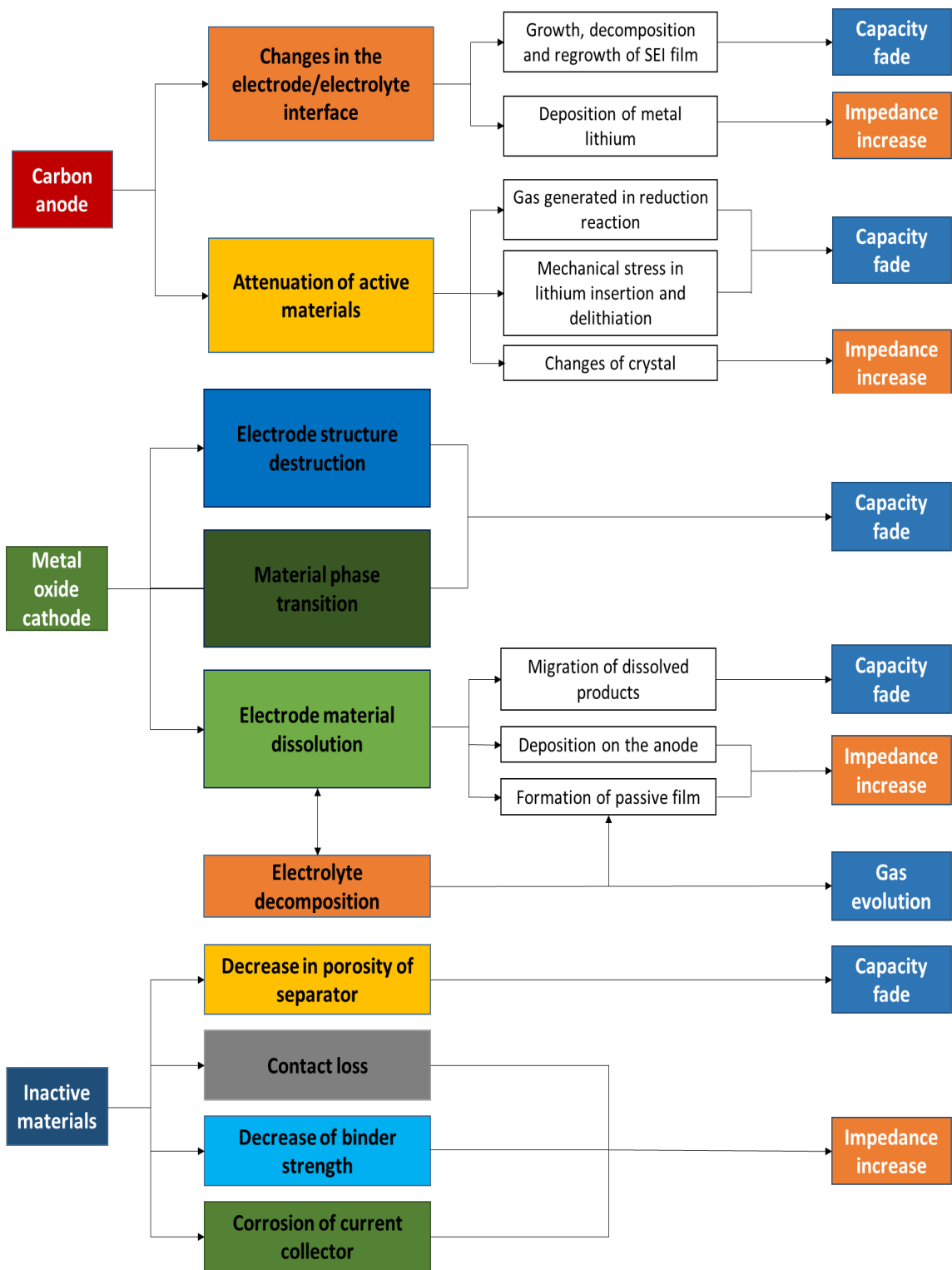


Figure 13 - Overview on aging phenomena

### ***1.7.1 Other factors affecting aging***

It has been observed that aging rate and consequently failure can be significantly influenced by external factors such as temperature, charge-discharge rate and depth of discharge.

#### **Temperature**

For lithium ions batteries the point of balance in terms of temperature seems to be 25°C, when the external temperature is higher the aging rate increase with increasing of temperature while for lower external temperature the aging rate increases as the temperature decreases. With temperatures less than 25°C lithium plating begins to be prominent and, at the same time, intercalation become harder favouring more and more lithium plating. In addition, safety problems begin to arise. For temperatures above 25°C, the thickening of SEI film and degradation of the cathode are the dominant reactions of battery aging. For example, at 45°C the capacity degradation rate caused by cathode degradation is 10 times higher respect to 25°C. High temperature causes the brittleness of SEI film, exhibiting high-density defects due to the film modification and by product formation such as gas despite the positive effect on the film growth. This characteristic leads to the degradation of anode performance.

#### **Charge-discharge rate**

The increasing charge-discharge rate is effective for accelerating battery aging. As the C rate increases, lithium plating and deposition occur on the anode surface, accompanied by structure attenuation. It is found that the effective capacity of the anode is the limitation of battery performance at high C rates. On the contrary, the cathode is less sensitive to high C rates, and even reaches an excellent status with the best reversible and rate ability at 3C, which can guide fast charging.

#### **Depth of discharge**

Unlike what you might think, it is the width of the discharge interval that accelerates degradation rather than the upper and lower boundary value of depth of discharge. When DOD is limited to 10%-70%, batteries degrade slower compared with DOD of 0%-100%. However, the influence of DOD on LFP and NMC batteries seems to be negligible compared with temperature and cycle time.

### 1.8 Solid Electrolyte interface

The Solid Electrolyte interface (SEI) layer is the primary source of degradation of batteries<sup>8</sup>. It is a passivating film that typically develops on the surface of anode which is electrically insulating yet provides sufficient ionic conductivity for lithium to intercalate into and de-intercalate out of the electrode particles readily<sup>2</sup>. The formation of the SEI is a set of reactions involving multiple components in the electrolyte, its development is caused by reaction between the electrolyte and the graphitic negative electrode and is roughly composed of the salt degradation products and the partial or total reduction products of electrolyte solvent. The SEI layer is mainly formed during the first charging cycle while it consumes around 5% of the active lithium ions<sup>4</sup> (this aspect has to be taken into consideration by the designer) and then it keeps growing slowly during aging of the battery causing an irreversible lithium consumption and a reduction of the energy that the battery can deliver<sup>3</sup>.

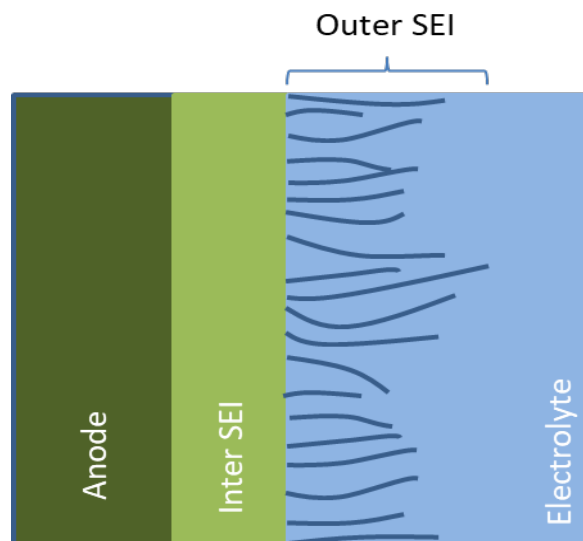


Figure 14 - Sketch of SEI film

This passive film formation has multi-layered structure, with a dense layer of inorganic components close to graphite electrode followed by a porous organic layer close to electrolyte. Furthermore, placing together the different layers of SEI, can cause an increase in the overall resistance of the battery, leading to an increase in temperature and, since Lithium ions are consumed, capacity fade. The temperature and the SOC plays an important

role in SEI composition and growth in fact high temperature leads to and additional SEI formation and capacity loss. Also, high SOC accelerate the SEI growth because high SOC means high concentration of ions on the electrode and a large potential difference between electrodes and electrolyte interface leading to chemical reaction, which age battery<sup>6</sup>.

How can SEI be seen in the results of tests?

As has been said, the SEI can causes an increase in the battery resistance and capacity face, so during our tests, we can expect to see an increase in temperature and also a little loss of capacity.

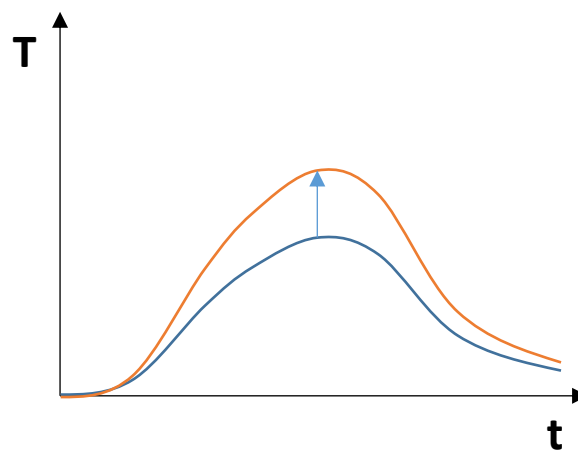


*Figure 15 - Increase in temperature due to SEI film*

### ***1.9 What is lithium plating***

A Lithium-ion cell that operate under normal condition does not contain metallic lithium. Under normal charging conditions, Lithium ions undergo intercalation reactions at both electrodes, shuttling from the galleries of the metal oxide positive electrodes into the galleries of the carbonaceous anodes upon charge and vice versa on discharge. So, normally, no Lithium plating is detected but under more strenuous conditions, deposition of metallic lithium can occur. Such conditions include low temperature, high charging rate and overcharging but also aspects of the battery design such as low anode/cathode ratio and manufacturing defects<sup>7</sup>. However, Li plating is kinetically favourable, as the working potential of graphite is very close to that of metallic Li deposition. Among various anode materials that are currently in use, graphitic anodes are more susceptible to lithium plating, due to the proximity of its reversible potential to Li, while coke, hard carbons and especially

lithium titanate anode are less susceptible to lithium plating<sup>14</sup>.

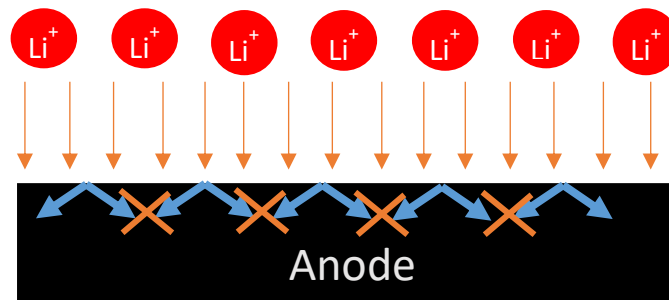


Figure 16 - Lithium ions have some difficulty to intercalate into the anode

The plated lithium is largely reversible and can be seen as a cyclic phenomenon but unfortunately, the effects of lithium plating do not disappear entirely during the discharge. It is possible that some of the lithium thus plated may re-oxidize during the subsequent discharge or intercalate ‘chemically’ into graphite, given sufficient time. In addition, lithium plating is known to be dendritic, often inducing internal shorts, which will pose serious problems in terms of reliability and safety.

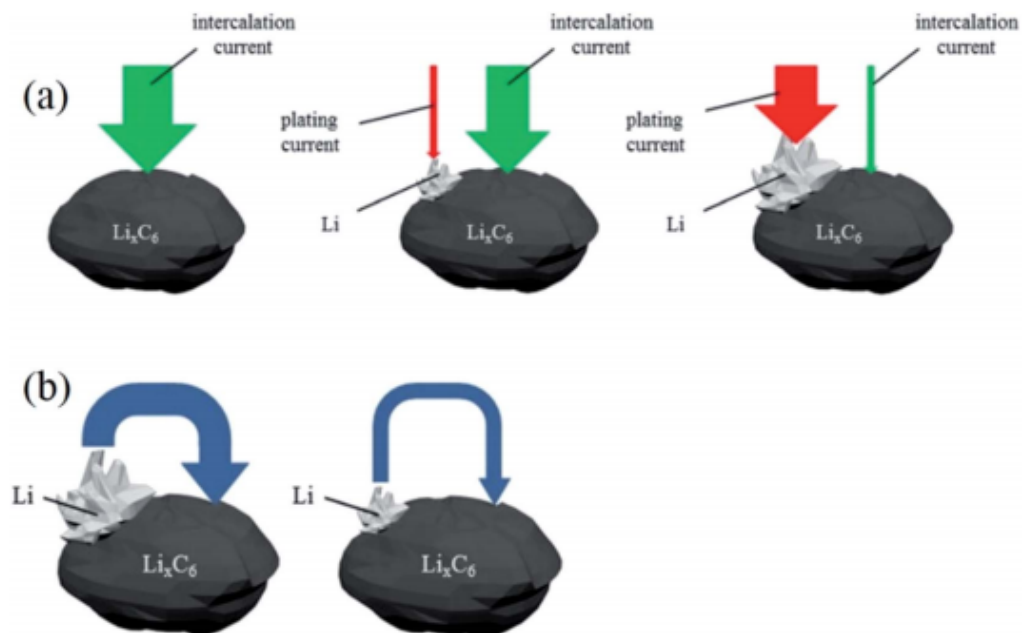
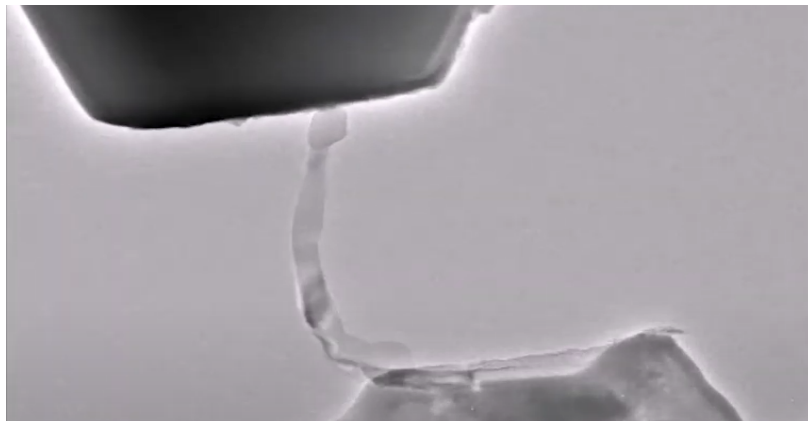


Figure 17 - Schematic of (a) the intercalation and plating currents during charging to higher states of charge and (b) the re-intercalation of deposited lithium during rest<sup>7</sup>

Apart from operating conditions of high charge and low temperatures, there are several cell design aspects that will accentuate the propensity towards Li plating. Anode materials that have high reversible potentials (more positive to Lithium), for example coke, will be less amenable for such lithium plating, while graphite with its reversible potential close to lithium deposition potential will be more susceptible. Further, the ratio of anode capacity to cathode capacity is a critical parameter. Li-ion cells generally have excess anode capacity compared to cathode, but a reduced amount of anode reserve will polarize the anode to lithium deposition potentials. The anode is required to be larger, not only in capacity, but also in area and dimensions to avoid edges that are prone to lithium plating. Finally, the nature of electrolyte is a critical parameter that can affect the intercalation kinetics and thus the plating behaviour<sup>14</sup>.



*Figure 18 - Dendrite growth between electrode and electrolyte (from Web)*

When anode lithium plating occurs during abnormal charging, the deposited metallic lithium reacts spontaneously with the electrolyte until an intact passivation film (SEI) forms. The reaction between metallic lithium and the electrolyte consumes the active lithium and electrolyte, which will induce capacity degradation and poor efficiency. Simultaneously, the formed SEI film increases the internal resistance of LIBs causing larger polarization during the intercalation/de-intercalation of Li ions. After anode lithium plating, partial deposited lithium, especially dendritic lithium, may lose electrical contact with the anode and may even form floating fragments or structures in the electrolyte (known as dead lithium) during the subsequent discharge. Both dead lithium and the formation of SEI film will result in permanent loss of active lithium and are responsible for fast capacity

degradation during anode lithium plating. It should be noted that anode lithium plating is a self-accelerating process, since the reaction of metallic Li with electrolyte leads to an increase of internal resistance due to thickening of SEI film and drying out of the electrolyte. The increased internal resistance enhances the likelihood of further anode lithium plating during the subsequent charging<sup>7</sup>.

### ***1.9.1 How to detect lithium plating***

Since Lithium plating affects the safety and the efficiency of Lithium-ion batteries, a lot of efforts have been put to develop effective methods to easily detect it and, in fact, actually exists a lot of electrochemical techniques (but also physical techniques) to reveal plating. The electrochemical ones involve anode potential technique, Columbic efficiency, stripping voltage and voltage relaxation.

The first technique is based on the fact that anode lithium plating emerges when anode potential drops below 0V and positioning a reference electrode into the Li-ion batteries anode potential can be seen as a difference in voltage emerges. To make this work, it is crucial that the introduction of a reference electrode should not interfere with the current distribution between the anode and the cathode of the battery itself; large size reference, for example, could disturb with the ionic pathways between anode and cathode, Also the position of the reference electrode may interrupt the current distribution and influence the accurate measurement of anode potential. However, the main disadvantage of this technique is that the built-in reference electrode requires modifications of the battery design and fabrication.

On the contrary, the Columbic efficiency calculation is not an invasive method. The Columbic efficiency is defined as the ratio of the discharge capacity to the charge capacity during one cycle and it is able to reflect side reactions such as SEI formation and electrolyte oxidation. Obviously, the Columbic efficiency will decrease when Lithium plating occurs because that cause a consume of active lithium forming dead lithium during discharging. In order to correctly execute this measurement, a high accuracy coulombmeter is needed. The only drawback is that other parasitic reactions may also result in a decrease of Columbic effect and if these reactions are severe the measurement could result invalidated.

At low temperature, after anode lithium plating occurs, there is a high voltage plateau during the subsequent discharge, which provides evidence of anode lithium plating in LIBs. This

high voltage plateau is attributed to the preferential oxidation stripping of deposited metallic lithium, due to its lower standard electrode potential compared with that of the intercalated  $\text{Li}_x\text{C}_6$ . This detection method of anode lithium plating is called stripping discharge. In addition to that, anode lithium plating has recently detected in situ by voltage relaxation during the resting of LIBs after charging at low temperatures. A mixed potential of the intercalated graphite phase and deposited metallic lithium reinserts into graphite phase and deposited metallic lithium reinserts into graphite even if no external current passes the LIBs.

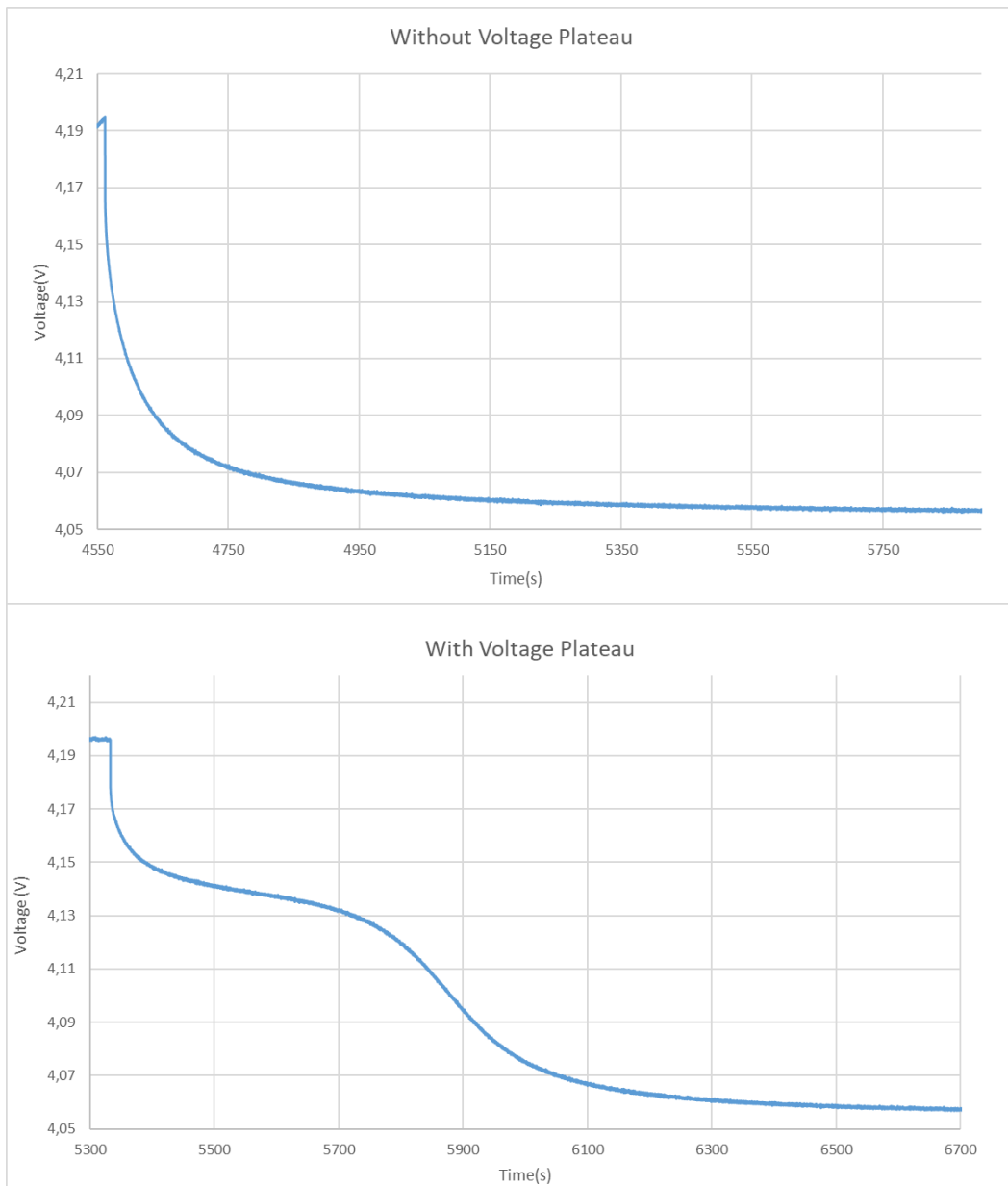


Figure 19 - Difference in voltage relaxation with and without lithium plating

# CHAPTER 2

## 2. Abuse case under analysis

### 2.1 Mechanism and degree of failure

Why accident involving batteries still occurs sporadically even if the battery can pass compulsory safety tests? The answers may come from two views:

- 1) the probability of the self-induced failure
- 2) the abuse condition in practical use

In the view of probability, the self-induced failure of the lithium ion battery exists but at a very low level. The abuse conditions can be categorized into mechanical abuse, electrical abuse and thermal abuse and often lead to thermal runaway as can be seen in Figure 20.

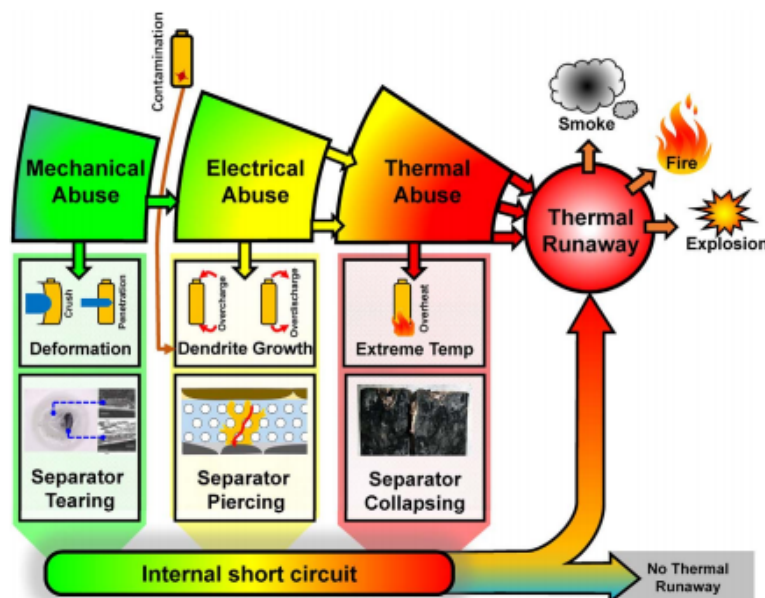


Figure 20 - Most common causes of thermal runaway<sup>15</sup>

The mechanical abuse (deformation and fracture of the separator caused by nail penetration or crush) can trigger short circuit, which is a common feature in the electrical abuse (the separator can be pierced by dendrite, the growth of which can be induced by overcharge and over discharge), whereas the short circuit releases heat and initiates a thermal abuse condition. Under a thermal abuse condition (shrinkage and collapse of the separator can happen), the battery is heated to extreme temperature and then undergoes thermal runaway.

Within the cell, different degree of failure can be encounter:

Soft short-circuit localized contact between electrodes. This phenomenon could be self-corrected due to melting of the region in contact. A battery with a SSC in it is still operational but it has a high self-discharge rate.

Hard short-circuit strong connection between electrodes that cause really high current flow and complete discharge, resulting in a voltage drop that lead to 0V and the whole cell become the resistance in the circuit. The battery turns out to be hopelessly damaged.

Explosion and fire: phenomenon powered by chemical reaction happening inside the battery. If the heat generated by these reactions is not removed quickly, a thermal runaway could happen, leading to fire and explosion<sup>2</sup>.



*Figure 21 - Explosion of battery due to abusive test (via Web)*

A massive internal short circuit, as can be seen in Figure 21, often caused by mechanical or electrical abuse, will directly trigger thermal runaway. However, also mild internal short circuit can happen, implying little heat and no thermal runaway at all because the energy releases depends on the degree of separator fracture.

## ***2.2 Thermal runaway mechanism***

The mechanism behind a thermal runaway is complex because due to a sequence of events, each of them with a specific influence, that gives the birth to a chain of reactions as shown in Figure 22. The chemical reactions happen in sequence one after another creating a loop called Heat-Temperature-Reaction (HTR) loop; the heat generation rises the temperature of the cell, starting the side reactions and these side reactions releases more heat, forming HTR loop. The HTR loop, with sufficient time and cycles, lead to thermal runaway. During the process of temperature rising, specific phenomena happens sequentially and those are: SEI

decomposition, reaction between anode and electrolyte, melting of the PE base, decomposition of NCM cathode and decomposition of the electrolyte. Once the separator collapse, the internal short circuit generated allows to release all the electric energy instantaneously, leading to a thermal runaway powered by the electrolyte.

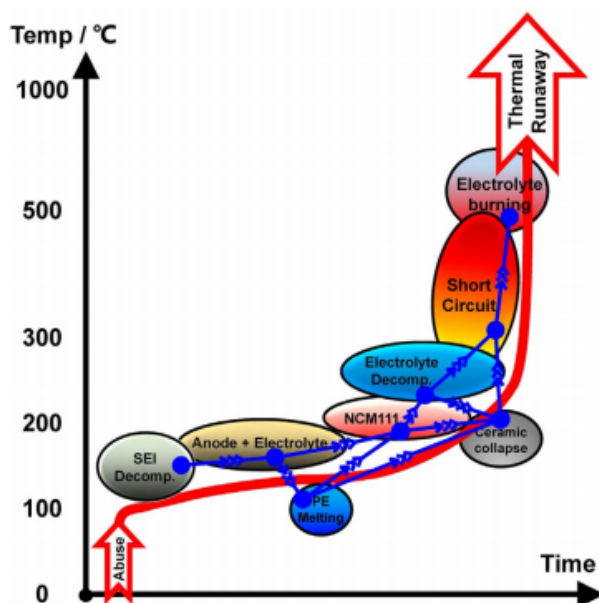


Figure 22 - Qualitative interpretation of the chain reactions during thermal runaway<sup>15</sup>

In order to have a combustion three elements are required: flammable fuel, oxygen and ignition source. The flammable fuel is sufficiently supplied by organic solved and the gas generated by the electrolyte decomposition instead oxygen and ignition source are not always guaranteed to generate thermal runaway. The oxygen released by the cathode decomposition is sometimes insufficient to support a complete combustion, therefore the combustion always occurs outside the cell after the flammable gases vent out. The ignition source instead is largely random, making the thermal runaway difficult to predict. However, the ignition source can be a spark resulted by the fierce friction between the high speed outflow and the vent valve or by the arc generated by the external short circuit during thermal runaway.

The reaction that occurs between anode and electrolyte during thermal runaway can be summarized into three steps; the first step is the initial decomposition of the SEI layer with an exothermic peak locates at approximately 100°C, the second step has a wide range of

temperature with a steady heat generation rate and the third step denotes the final decomposition of the graphite anode with the electrolyte at higher than 250°C.

Rising temperature are also extremely dangerous when it reaches the melting point of separator. The commonly used base material for current commercial separator are PE (polyethylene) and PP (polypropylene) with melting points respectively of 130°C and 170°C. The separator melting is an endothermic process and the temperature increase rate will thus slow down. The holes in the separator will be closed during melting, making it difficult for the lithium ion to transfer inside the cell. Hence, the separator displays a shutdown effect with a sharp increase in the cell resistance. After the shutdown, as the temperature increase, shrinkage of separator follows. The separator of the cathode and anode will lose due to the area diminish after separator shrinkage. The internal short circuit will occur once the cathode and anode contact together after the shrinkage of the separator. The collapse of the separator follows the shrinkage when the temperature is so high that the separator melts. The internal short circuit caused by shrinkage can be so massive that the separator collapses quickly, whereas the internal short circuit can also be mild and the separator may collapse much later.

### ***2.3 Thermal abuse***

Local overheat is a possibility when a thermal abuse condition occurs in a battery. If mechanical and electrical abuses are not taken into account, a typical cause of overheat can be caused by contact loose of the cell connector<sup>15</sup>. This condition can be caused, for example, by manufacturing defects and lead to an increase in battery resistance with intensive heat generation in a particular area, resulting in local overheat and thermal runaway. Heat can come from internal short circuit because of Joule heating ( $I^2R$ ) until the battery begin to produce heat by internal chemical reaction. Overcharge can also be a cause of heating due to other oxidative chemical reactions that can trigger thermal runaway. During those situations, response of cell can be characterized as falling into three major temperature regimes as can be seen in Figure 23.

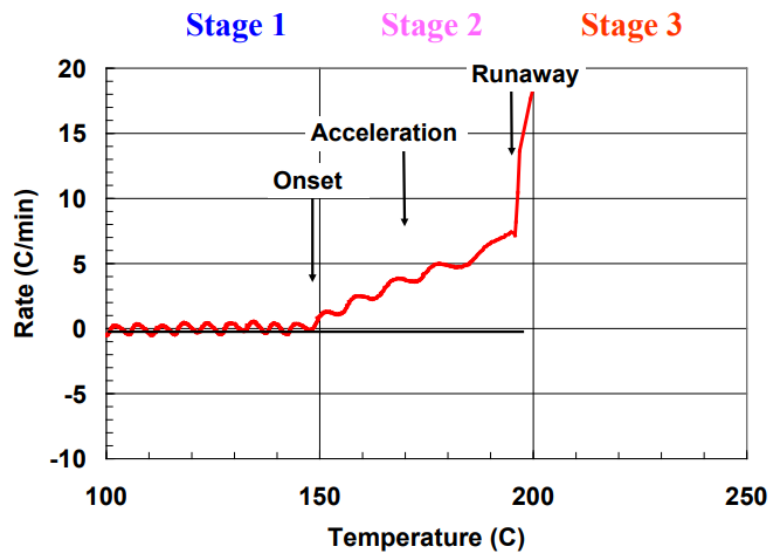


Figure 23 - Different stages of temperature response<sup>9</sup>

During normal operation of battery, the self-heating rate is  $0.2^{\circ}\text{C}/\text{min}$  and this low heat generation can be re-absorbed by the battery itself (Stage 1). If the heat rise (for example due to abuse), the battery pack is not able to accommodate the heat in itself and temperature will continue to rise due to sustained exothermic reactions (Stage 2). Addition heating promoted by accelerating chemical reactions causes the cell to enter in Stage 3 resulting into a thermal runaway. Thermal runaway is defined as a self-heating of  $10^{\circ}\text{C}/\text{min}$  or greater.

## 2.4 Electrical abuse

### External short circuit

The external short circuit forms when the electrodes with voltage difference are connected by conductors. The external short circuit of the battery pack can be caused by deformation during car collision, water immersion, contamination with conductors, or electric shock during maintenance. Comparing with penetration, the heat released on the circuit of external short does not heat the cell. In terms of current, a behaviour peak-plateau, drop can be a hint that an external short circuit is happening. Although some heat is released on the external circuit, the high peak current could lead to fast temperature rise and cell swell, which are dangerous. The swell indicates that gas is generated during external short circuit. The over temperature is caused by the ohmic heat generation during short circuit and the peak value of current is restricted by the diffusion of lithium ion in the anode, and so either by

increasing the mass transfer coefficient for lithium ion in the anode or increasing the surface area of the anode allows for higher currents with more rapid heating of the battery during external short circuit.

### ***Overcharge***

The overcharge induced thermal runaway can be way more dangerous than the other abuse conditions because excessive energy is filled into the battery during overcharge. The failure of the battery management system to stop the charging process before the upper voltage limit is the ordinary cause of overcharge abuse. The inconsistency with the battery pack determines that the cell with the highest voltage is the first overcharged cell, followed by the others. The heat and gas generation are the two common characteristics during overcharge. The heat generation comes from ohmic heat and side reactions. It has been observed that the amount of heat generation has a positive correlation with the charging current, indicating that the ohmic heat is one major heat source during over-charge. The outcome of overcharge varies with the test conditions. The cell exploded under high current, whereas only swelled under small current.

### ***Over discharge***

The discharge is another possible electrical abuse condition. Once the BMS failed to monitor the voltage of any single cell, the cell with the lowest voltage will be over discharged. The cell with the lowest voltage in the battery pack can be forcibly discharged by the other cell connected in series during over discharge. During the forcible discharge, the pole reverses and the voltage of the cell becomes negative, leading to abnormal heat generation at the over discharged cell. The over discharge can cause the capacity degradation of the cell. During the process of over discharge, the over de-lithiation of the anode causes the decomposition of SEI, which will produce gases like CO or CO<sub>2</sub> resulting in the cell swell.

## ***2.5 Mechanical abuse***

Destructive deformation and displacement caused by applied force are two common features of the mechanical abuse. Vehicle collision and consequent crush or penetration of the battery pack are the typical conditions for mechanical abuse. It can be a puncture, a crush, a vibration or a shock or, however, a strong pressure on the battery's envelope. This

kind of phenomenon is quite possible during car collision. The deformation of the battery pack may result in dangerous consequences: 1) the battery separator gets torn and the internal short circuit (ISC) occurs; 2) the flammable electrolyte leaks and potentially causes consequent fire<sup>15</sup>. Penetration is another common phenomenon that may occur during the vehicle collision.



*Figure 24 – Example of denting on a pouch battery*

Comparing with the crush conditions, fierce ISC can be instantaneously triggered when penetration starts. The mechanical destruction and electrical short occur simultaneously and the abuse condition of penetration is more severe than that of simple mechanical or electric abuse.

## ***2.6 Mechanical abuse test***

Various test has been developed to evaluate the safety of Li-ion batteries under mechanical deformation. The techniques to induce internal short circuit on fully assembled cells are nail penetration, indentation and pinch tests. This kind of tests try to reproduce the damage that a normal use for automotive purpose could create under specific circumstances. So, the purpose is to create a small break in the separator mimicking the very rare internal short circuit event as in Figure 25.

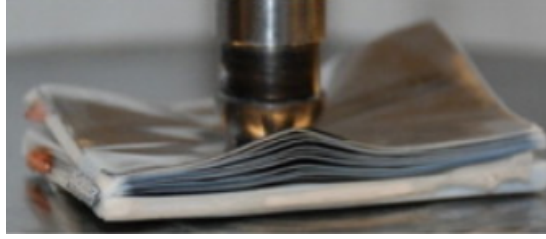


*Figure 25 – Example of indentation test*

Test like nail penetration will cause for sure an internal short circuit because the battery, when we reach the end of the test, results to be completely pierced by the nail as can be seen in Figure 27. When attempting to replicate a scenario in which a cell undergoes an internal short circuit, the nail penetration test is unsuitable due to it being inherently intrusive, spreading the short circuit across a large area and multiple layers, and introducing a heat sink at the region of initiation. For these reasons, the nail penetration test is not considered to be a suitable technique for reproducibly inducing in-field failures or worst-case scenarios. Inducing an on-demand local failure within the cell that is representative of an in-field failure poses a great challenge.



*Figure 26 – Example of pinch test*

On the contrary, tests like pinch and indentation (only if the tip does not cross a certain threshold of deepness inside the structure of the battery) can be used as non-disruptive tests. This means that there is a high possibility not to have internal short circuit allowing to study

phenomena that act on the battery during damage but granting at the same time the operational integrity of the cell.

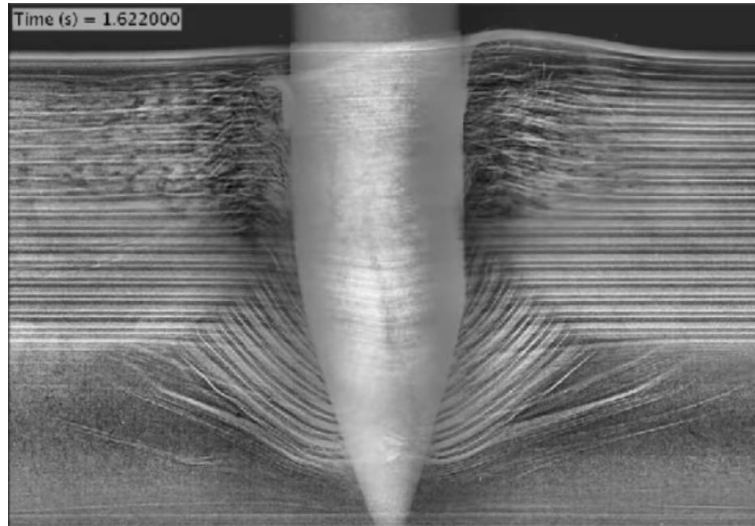


*Figure 27 - Cross-section view on nail penetration*

### ***2.7 Internal behaviour during mechanical abuse***

Try to map the exact behaviours of internal arrangement changing after a penetrative test is quite difficult since the destructive nature of the mechanical abuse and the violent response that those tests generate. However, after many studies that had employed non-destructive procedure like X-ray tomography, neutron imaging and in-situ analysis we have a discrete idea of what happens at each component.

- Tearing of current collectors: current collectors under the indenter are discontinuous, showing evidence of cracking and tearing
- Through layer cracking (fault lines): shear-type faults span multiple-layers and are oriented at approximately a 45° angle.
- Kinking of layers: correlated kinking extending for multiple layers from the indenter.
- Local melting: small black voids without original materials<sup>11</sup>.

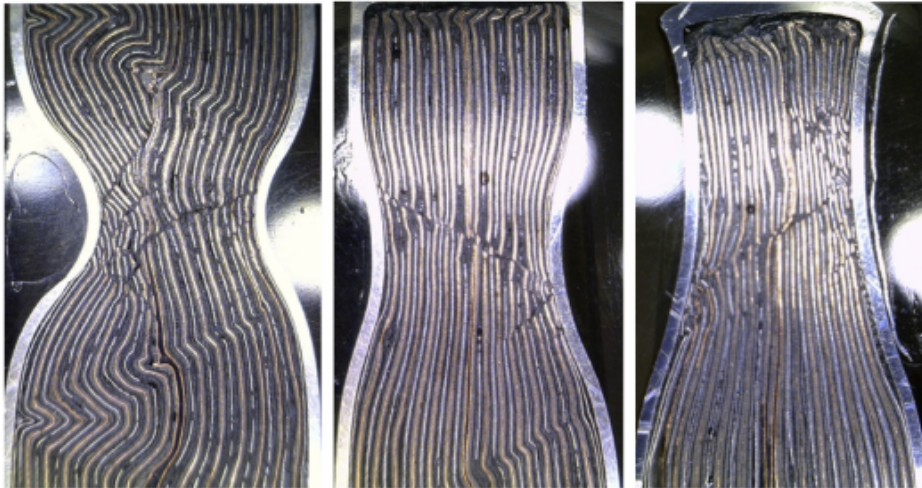


*Figure 28 - Internal deformation of Li-ion cells after pinch tests.*

The tearing of current collectors and shear faults are prominent features of deformation. The tearing triggered fault through the layers and shifting of the electrode materials. Spacing between layers also started to decrease and the stresses on the current collectors were released with increased stretching of the separator. We can see some recursive behaviours in the jellyroll response to crushing:

- a) Initial homogeneous compression of the jellyroll: deformation is distributed according to the compliance of each layer. The displacement field is homogeneous and determined by the shape of the indenter.
- b) Fault formation: increased loading eventually exceeds the strength of the jellyroll resulting in a localized fault formation.
- c) Materials flow and internal rearrangement: electrode materials near the fault line will flow around the torn current collectors and may slide into the fault. Since control of the external loading is based on the rearrangement of material, it may temporarily relieve the external force.
- d) Separator failure: separators are stretched and twisted to conform to the faults and eventually exceed the failure point, resulting in internal short circuit as opposite electrode material and pieces of current collectors come into contact.

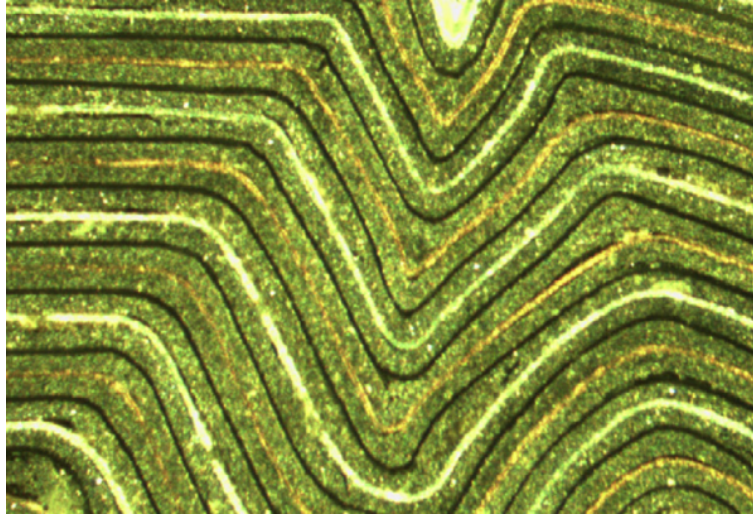


*Figure 29 - Cross section image of Li-ion cell pinched*

The sequence of deformation mechanisms and events leading to internal short circuit is assumed to be this: the pressure on the battery creates a displacement field and distributes through-thickness deformation according to the compliance of each layer. With continuous indentation, deformation localizes into successive cell layers closest to the indenter. The separator layer eventually fails by the intrusion of deformed electrodes and exposes electrodes of opposite polarity to each other and this create the internal short circuit.

### ***2.8 Separator mechanical properties***

As already said in the introduction, in this work of thesis only non-disruptive tests will be executed. This means that internal hard short circuit will not happens and the electrodes will not touch each other; this condition, intrinsically, suggest that the separator will not broke<sup>12</sup>. Due to its porous microstructure and mechanical properties, the separator probably does not strongly contribute to the structural response of the jellyroll. It can stretch much more than metal foils, so we can expect it to break after them, creating an electrical short. Standard polymer separators are composed of polyethylene and polypropylene layers with a yield strength of approximately 10-40 Mpa, which is significantly lower than the yield strength

of the metal current collectors or the ceramic electrode materials.

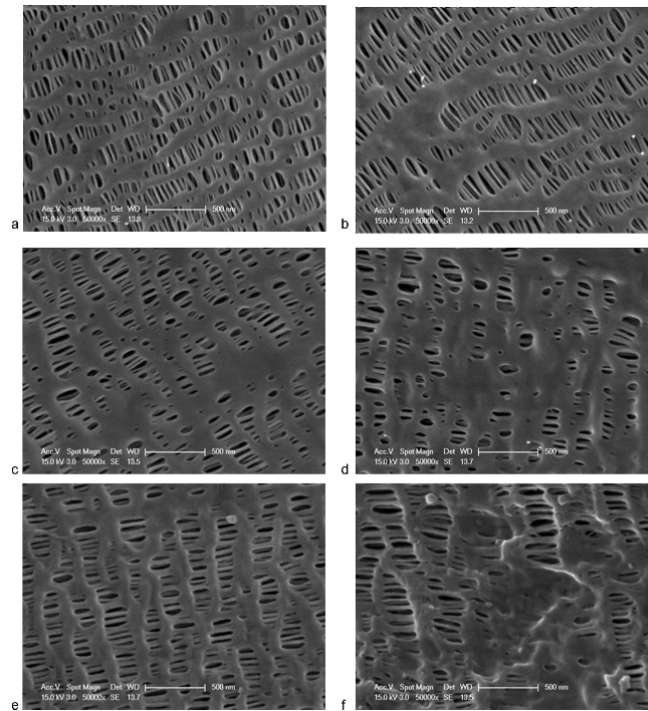


*Figure 30 - SEM characterization of separator membranes after compressive stress testing*

Direct application of stress to the battery stack would induce creep in the separator as result of stress accommodation since the cells are packaged in flexible aluminium-laminate foil pouches. The cell capacity decreases with increasing stress and corresponding total separator strain; the observed capacity losses occur as pore closure decreases the number and size of pathways for ions to shuttle between the electrodes during charging and discharging. This limits the ability of ions to reach reaction sites at a given charge/discharge rate and thus limits the amount of energy that is stored/used. Mechanical deformation of the electroactive separator can cause an apparent decrease in cell capacity by limiting ionic transport and increasing the internal resistance of the cell.

# CHAPTER III

## *3. Test design*

### *3.1 Purpose of the tests*

The objective of this work of thesis is to give a research contribution to the understanding of the hazard conditions of Li-ion batteries under the case of ‘non-critical’ mechanical load. In particular, phenomena of interest will be heat generation, voltage variation and changing in voltage relaxation. The first two behaviours were taken into account to have a chance to answer the first big question of this research: a battery pack slightly damaged can be used again or need to be replaced entirely? Temperature and voltage variation can be used as reliable information about internal behaviour of a Lithium-ion battery; if temperature is too high or a voltage drop happens, it could mean that an internal short circuit could be in progress and the battery needs to be replaced. However, if we executed correctly all the tests in a way to obtain only non-disruptive damage, we excluded a priori hard short circuit as response but, it has to be noted that, soft short circuit could happen anyway.

On changing in voltage relaxation, caused by Lithium plating, it is necessary to spend a few more words. In the first chapter it has been said that Lithium plating is an irreversible phenomenon due to the aging of batteries that affects negatively their efficiency; in addition, the two main causes of it have been identified in low temperature and high charging current. Nevertheless, in the second chapter, we also said that during mechanical load, there is a good chance to have a thermal response coming from the battery, so, it is probable that two behaviours in opposite direction for what regards Lithium plating growing ( $\uparrow$  high charging rate and  $\downarrow$  increase in temperature) will be seen. Moreover, if we will not have appreciable temperature raising, a correlation between mechanical load and Lithium plating changing could be introduced.

### *3.2 Battery under test*

All the batteries used were 41 Ah Lithium ion pouch cell with cut-off voltage limits of 2.5 V and 4.2V, disassembled from a battery pack containing 24 identical battery modules. Twelve of the modules were positioned horizontally in the front of the battery pack while the others twelve were arranged vertically in the back of the battery pack.



Figure 31 - Example of battery under test

In Figure 32, the layer arrangement can be seen. The battery reveals to contain 22 anode layers, 21 cathode layers and 44 separator foils and the two outermost layers on both side of the battery are anodes. This last information suggest that the active material deposited on the outer side of the last copper foil remains electrochemically inactive and do not participate in the charge transfer and the energy storage process.

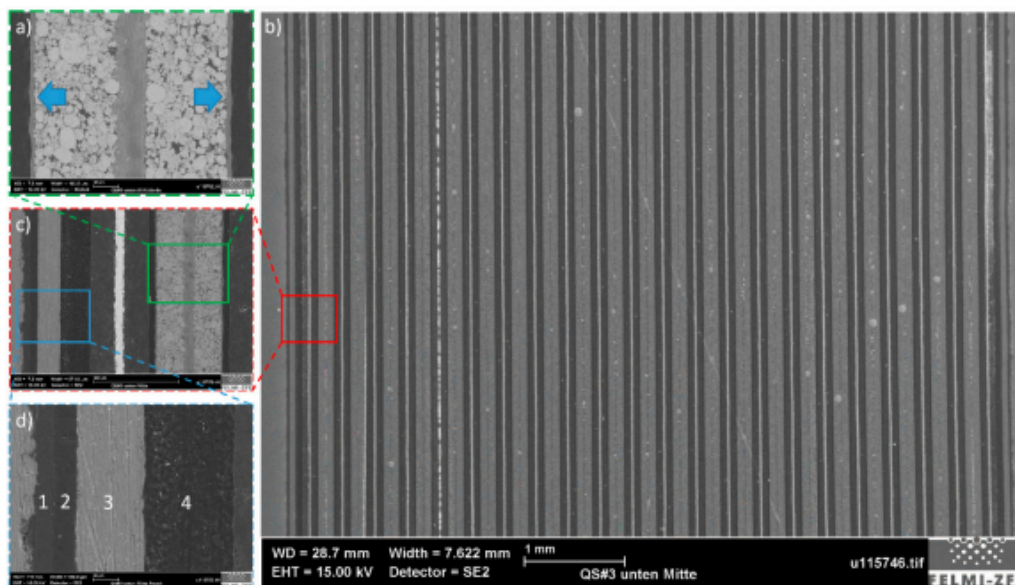


Figure 32 - Microscopic view of internal layers arrangement of the battery

In addition, the pouch is made of four layers of metallic polymer compound, specifically one Aluminium layer and three polymer layers. The overall thickness and composition of

the layers can be described as follow: 140 $\mu\text{m}$  for the anode layer that comprised 20  $\mu\text{m}$  of current collector and 60  $\mu\text{m}$  of active material on both sides made of graphite; the cathode instead, is 20  $\mu\text{m}$  wider than the anode due to its thicker current collector (25  $\mu\text{m}$ ) and active material (about 65  $\mu\text{m}$ ) made of a blend of NMC and LMO chemistries. The separator, made of fibres of PP/PE material, aligned in a direction perpendicular to the battery tabs, was evaluated around 20  $\mu\text{m}$  while its fibre thickness is around 3  $\mu\text{m}$ , as indicated from Figure 33.

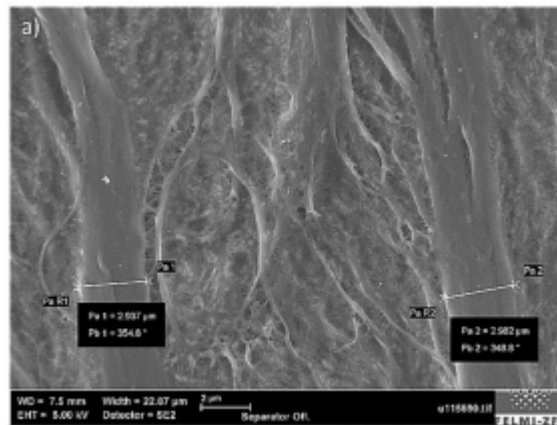


Figure 33 - Microscopic view of the separator

All the information about the thickness of the involved layers are report in the following Table. The tolerance of the measures is about 5  $\mu\text{m}$  and depends on the active material grain radius.

### 3.3 Structure of tests

Our idea for the development of tests was to design mainly two tests:

- In the first test, a thermal response had to be highlighted, so, we performed the electrical cycling of the batteries in order to have that kind of wanted reaction.
- In the second test, Lithium plating wanted to be observed, so, using information coming from previous test, it was performed an *ad hoc* electrical cycling.

The first problem that had to be resolved was grant truthfulness on test and excluded that output data were the results of some manufacturing defects; we needed to be sure that data were reliable and in order to do that, repeatability had to be granted.

Repeatability is a measure of the likelihood that, having produced one result from an experiment, you can try the same experiment, with the same setup, and produce that exact same result. It is a way for researchers to verify that their own results are true and are not just chance artefacts. To demonstrate a technique's repeatability, the conditions of the experiment must be kept the same. These include: location, measuring tools, other apparatus used in the experiment, observer, hypothesis and time period<sup>16</sup>. In order to accomplish that, the series of tests has to be repeated on a multiplicity of batteries and, if the event occur in all the tests, the result can be taken for reliable. For this thesis, three batteries were used during the tests.

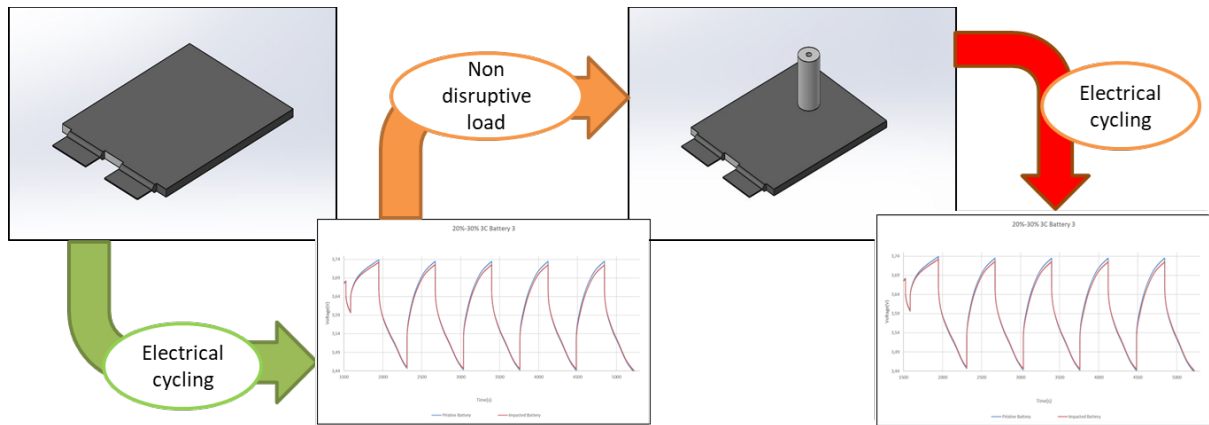


Figure 34 - Scheme of Tests

To add another layer of safety on the data of the tests, tests were executed with the following scheme:

- 1) Perform all the needed tests on the pristine battery.
- 2) Apply the tip to cause the wanted abuse
- 3) Perform the same tests on the impacted battery.

Doing this, the only data compared (pristine-damaged) are coming from the same battery and, in this way, the offset in voltage generated by, for example, manufacturing defects does not influence the comparison since it is equal for the same battery.

Once explained the scheme behind each test, we can finally discuss the operative condition of tests in terms of State of Charge (SOC), C-Rate and number of cycles.

Battery Condition	C-rate	State of Charge	Cycles	Repetitions
Pristine	1C, 2C, 3C	20%→30%	5	3
Pristine	1C, 2C, 3C	0%→90%	1	3
Impacted	1C, 2C, 3C	20%→30%	5	3
Impacted	1C, 2C, 3C	0%→90%	1	3

*Table 1 - Table of executed tests*

The range of State of Charge between 20% and 30% was chosen to maximize the possible response of the battery in terms of heat generation; this because the lower the SoC, the higher the resistance of the battery. In addition, the range of charge/discharge cannot be too low because we do not want to switch the control mode. To explain that, a small step back is needed; during, for example, a charging cycle, the battery is first charged at a fixed C-rate (usually 1C-rate, that, in case of the considered cell corresponds to 40A). The constant-current charge (CC) is enabled till the upper cut-off voltage limit is reached (4.2V).

At this point, the battery cell continues to be charged in constant-voltage mode (CV), so, the voltage is kept constant to its maximum value of 4.2v, while the current decays exponentially till a certain C-rate, usually  $C/40^2$ .

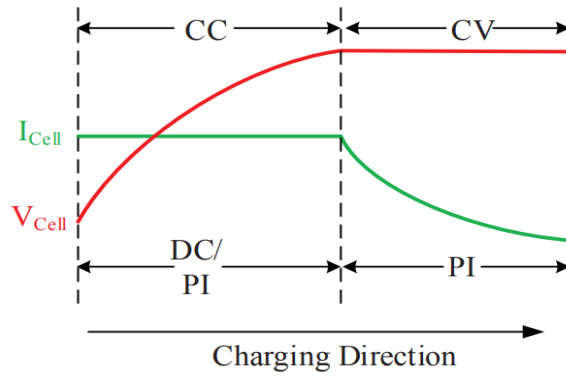


Figure 35 - CCCV charging method

After a relaxation time of 10-15 minutes, the battery is ready to be discharged at the desired C-rate. The discharge is stopped when the lower cut-off voltage (2.5V) is reached. So, in order to perform the entire experiment in constant current mode (CC), we did not go down further than 20%, value chosen as safety limit. This choice is important also for another reason: since for the electrical cycling between 20% and 30% five cycles are expected, working with constant current (CC) make also the programming of the battery tester easier.

Number of Step	Command	Current intensity [Ampere]	Control mode
1	Charge	40	Time → 720s
2	Wait	-	Time → 60s
3	Charge	40	Time → 360s
4	Discharge	40	Time → 360s
5	Charge	40	Time → 360s
6	Discharge	40	Time → 360s
7	Charge	40	Time → 360s
8	Discharge	40	Time → 360s
9	Charge	40	Time → 360s
10	Discharge	40	Time → 360s
11	Charge	40	Time → 360s
12	Discharge	40	Time → 360s
13	Discharge	40	Current ≤ 2A

Table 2 - Example of steps of charge/discharge programmed on battery tester for electrical cycling 20%/30%

In the specific situation of cycling between 20% and 30%, we calculated the time needed to reach 20% and then the time needed to gain another 10%. Starting by programming the 1C cycle, knowing that the battery has a maximum of 40Ah, one hour will be needed to reach 100% but, since we wanted to start our test at 20%, one fifth of an hour will be enough, so 720 seconds. In this way, we can start our test at 20%. Then, we needed to create a cycle with waving of  $\pm 10\%$  and, in this case, regular intervals of 360 seconds (tenth of an hour) of charging and discharging are needed. This last cycle was repeated five times. Last, after each test, the battery needed to be completely discharged; for this requirement, a time control was no more sufficient, so, a current control was exploit by the condition of current  $\leq 2.0$  A. Reaching 2.0 Ampere means to reach a C-rate of C/20, rate after which the battery is assumed to be completely discharged (State of Charge assumed to be equal to 0%).

The range of State of Charge between 0% and 90% was chosen to have a better chance to observe the phenomenon of Lithium plating. In the first chapter was said that Lithium plating has a cyclic behaviour, meaning that the film is formed during charging and then is erased (or at least reduced) during discharging. This involves that if we charge the battery, Lithium plating should still be here. The test steps, then, were the following: in order to reach the 90% of SoC, a ninth of hour was needed (3240 seconds) with a current of 40A (for 1C-rate) followed by half an hour with no current introduced in the battery. Doing this, we were able to see the voltage relaxation for thirty minutes and the eventual voltage plateau caused by Lithium plating.

Number of Step	Command	Current intensity [Ampere]	Control mode
1	Discharge	40	Current $\leq 2A$
2	Charge	40	Time $\rightarrow 3240s$
3	Wait	-	Time $\rightarrow 1200s$
4	Discharge	40	Current $\leq 2A$

*Table 3 - Example of steps of charge/discharge programmed on battery tester for electrical cycling 0%/90%*

The choice of the range was made using a previous study of the hosting institute (Vehicle Safety Institute) on Lithium plating for different State of Charge at low temperatures. During that research executed at 10°C, four different ranges were investigated: 0%  $\rightarrow$  70%,

0%→90%, 30%→90%, 70%→90% and it was found that the best range to appreciate Lithium plating was 0%-90%. On this basis, also in this test 0% to 90% was chosen as range to study Lithium plating.

Each test was also executed at different C-rate for different reasons. For cycling between 20% and 30%, a variation of C-rate till 3C will grant, for sure, a harder thermic response while for 0% to 90% test, we already said how Lithium plating is charging rate dependent and we wanted to explore this dependency.

### 3.4 Assembly design

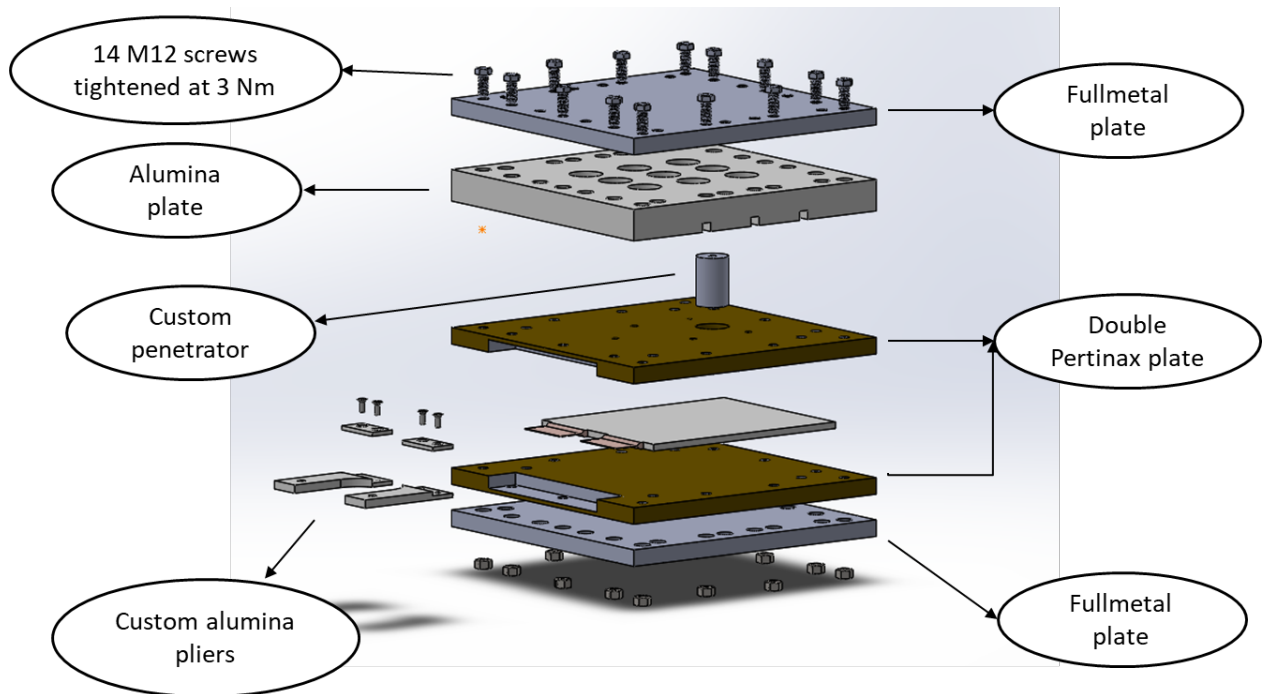


Figure 36 - Exploded view of the assembly

To accomplish the desired deformation on the battery several materials were employed as shown in Figure 36:

- Two full metal plates;
- One aluminium plate;
- Two Pertinax plates;
- Two custom aluminium pliers;

- Fourteen M12 screws;
- One custom penetrator.

All those materials were combined together to create a ‘‘sandwich’’ and be able to generate the impact. The aluminium plate was used to fix the centre of the impact and to maintain still the body of the penetrator; instead the two external full metal plates were held together with M14 screws and then proportionally compressed together in order to let the penetrator impact the battery.

### ***3.5 Penetrator design***

The design of penetrator and consequently of the penetration is the focal point of this test and also the most difficult issue to be addressed because a non-disruptive abuse was needed but a damage sufficient to have an interesting response in output data was requested.



*Figure 37 - Five punch heads used in indentation tests<sup>18</sup>*

Three main area can be treated in tip design and those are its width, its shape and the material it is made of. All these characteristics required a careful design in order to accomplish the wanted type of impact. As can be seen in Figure 37, several shapes can be employed in order to achieve different types of mechanical abuse; those showed in Figure are, from left to right, a 90° conical punch, three hemispherical punches with different diameters and a flat cylindrical punch. The deformation process caused by the utilization of those heads' shape is equal for all of them and can be described by three stages interspersed by two characteristic points (the inflection points and the peak force point) as shown in Figure 37.

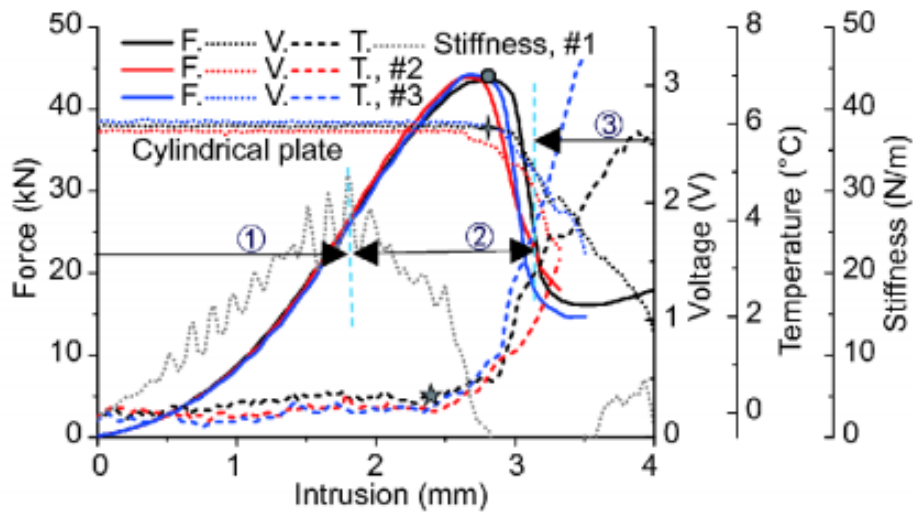


Figure 38 - Force, OCV and local temperature increase versus intrusion curves of a pouch cell under flat-end cylinder indentation<sup>18</sup>

In Stage 1, the force increases steadily with the increase in the stiffness before the inflection point (point determined by the maximum stiffness). In Stage 2, the force increase with decreases in the stiffness and the damage starts to accumulate leading to a global mechanical failure; Stage 2 can be also seen as a damage propagation process. In Stage 3, the force rapidly falls leading to global failure. This kind of distinction holds for all the indentation tests including lateral indentation of a cylindrical cell, flat-end cylinder indentation and hemispherical head indentation of a pouch cell and prismatic cell. It is important to understand which shape cause an Internal Short Circuit in the faster way and then choose the more conservative one for the designed tests. Different behaviours were observed regarding the different shapes of the impactor:

- 1) under flat-end cylindrical indentation, the temperature increases and OCV drop precede the peak force as shown in figure 37;

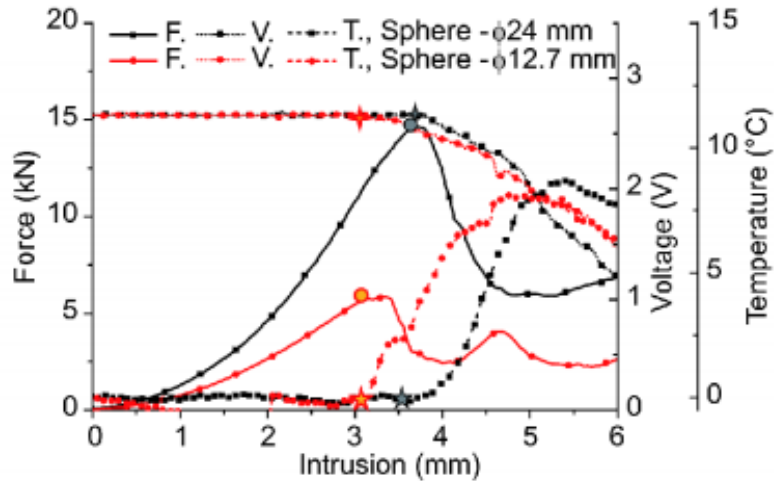


Figure 39 - Force, OCV and local temperature increase versus intrusion curves of a pouch cell under hemispherical head indentation<sup>18</sup>

- 2) Under hemispherical head indentation of a pouch cell, the peak force, OCV drop and temperature increase coincide with each other, as shown in Figure 38;

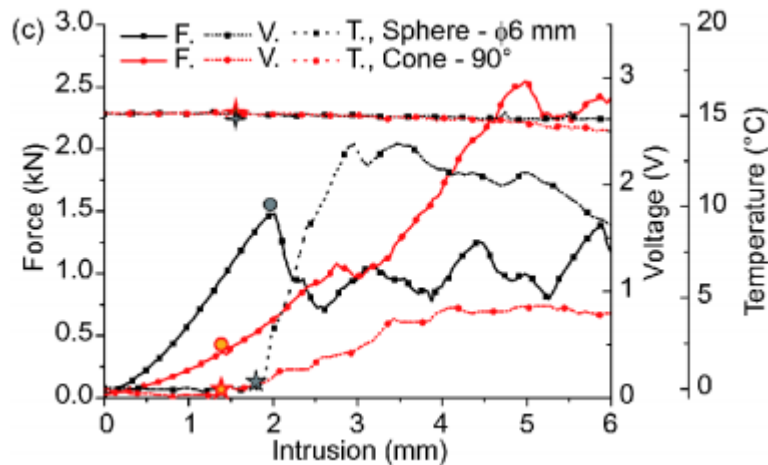


Figure 40 - Force, OCV and local temperature increase versus intrusion curves of a pouch cell under conical head indentation<sup>18</sup>

- 3) Under conical head indentation as shown in Figure 39, the OCV slowly decreases and shows a negligible drop although the tested sample can be already declared mechanically failed.

To have a quantitative measurement in order to classify the impactors from the most conservative to the less one, a good strategy is sort them by relative intrusion, as shown in Figure 40. The relative intrusion is calculated by dividing the intrusion by the thickness of the cell. Sorting them by relative intrusion at Internal Short Circuit, suggested by the

temperature increase, we obtain the following order:  $\phi 24$  mm hemisphere  $\rightarrow$   $\phi 12.7$  mm hemisphere  $\rightarrow$  flat- end cylinder  $\rightarrow$   $\phi 6$  mm hemisphere  $\rightarrow$  cone.

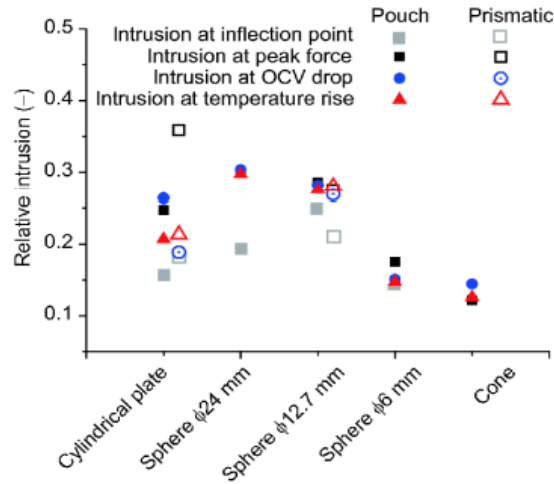


Figure 41 - Relative intrusion at inflection point, peak force point, OCV drop and temperature increase in the pouch cell and prismatic cell under different loadings<sup>18</sup>

It is clear how the decision about the shape inclines towards the hemispherical impactor. However, the relation between diameter of the hemispherical impactor and response of the battery still needs to be clear. In order to clarify this relation, three hemispherical impactors with different diameters were taken in account<sup>19</sup> and their response (in terms of rise in temperature, voltage drop and maximum load) until ISC in a mechanical load test were evaluated. For load-displacement curves, there was a progressing pattern meaning that the peak load at short circuit increased as the diameter increased, as can be seen in Figure 41.

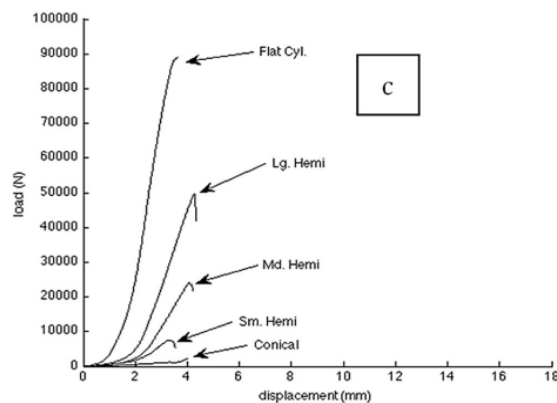


Figure 42 -. Load-displacement curves for small, medium and large hemispherical impactor<sup>19</sup>

Also, for what concerns voltage drop, small, medium and large hemispherical impactors create short circuit at later point, respectively, as can be seen in Figure 42.

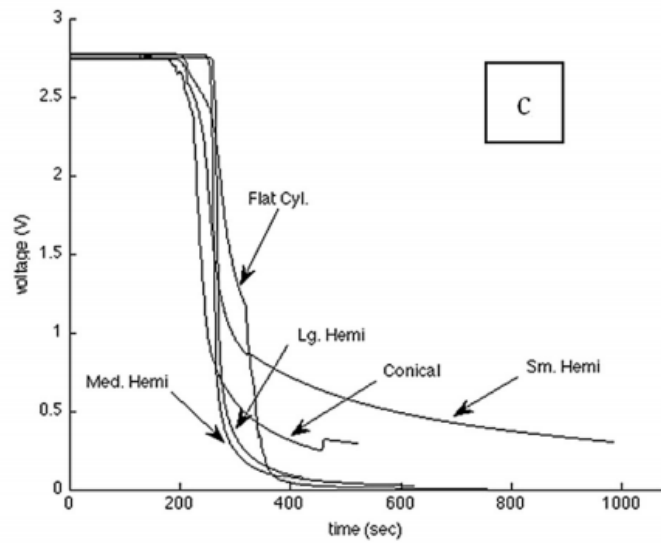


Figure 43 - Drop voltage for small, medium and large hemispherical impactor<sup>19</sup>

Peak load at short circuit is almost linearly increasing with an increase in punch diameter<sup>19</sup> as can be seen in Figure 43.

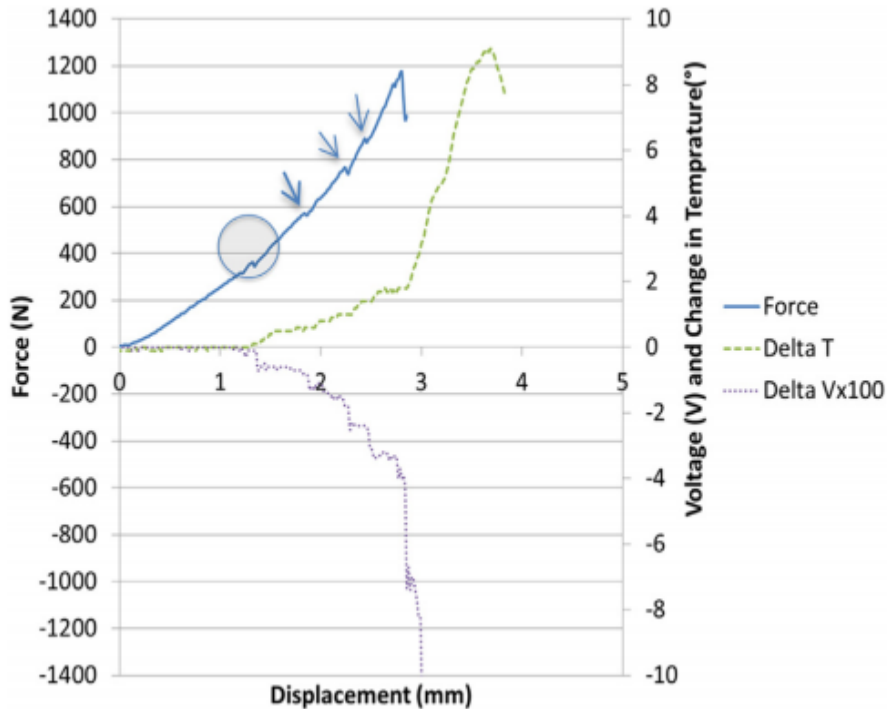


Figure 44 - Peak load (left) and deformation depth (right) at short circuit versus the diameter of the punch<sup>19</sup>

This means that the bigger the radius, more the ISC will be postponed, up to compression between two flat plates (which corresponds to infinite punch radius) where no ISC was observed. In light of this, it appears clear that the choice of penetrator's shape should lie with a hemispherical head but about the diameter there are still several ways possible. This because combining the information coming from Figure 32 and Figure 34, the greater the diameter of the punch, the higher the peak load but, at the same time, the greater the displacement of the intrusion inside the battery before a ISC event. This means that, most likely, exists an exact trade-off between the diameter of a hemispherical punch and the maximum intrusion in a battery (without causing an ISC). In the guest Institute (VSI), a test with a 30mm hemispherical impactor was already performed in order to study the response in different contact points of the battery, as shown in Figure 46. The test was performed until the ISC was reached and this can be helpful to understand the operational limit in terms of maximum deepness reachable.

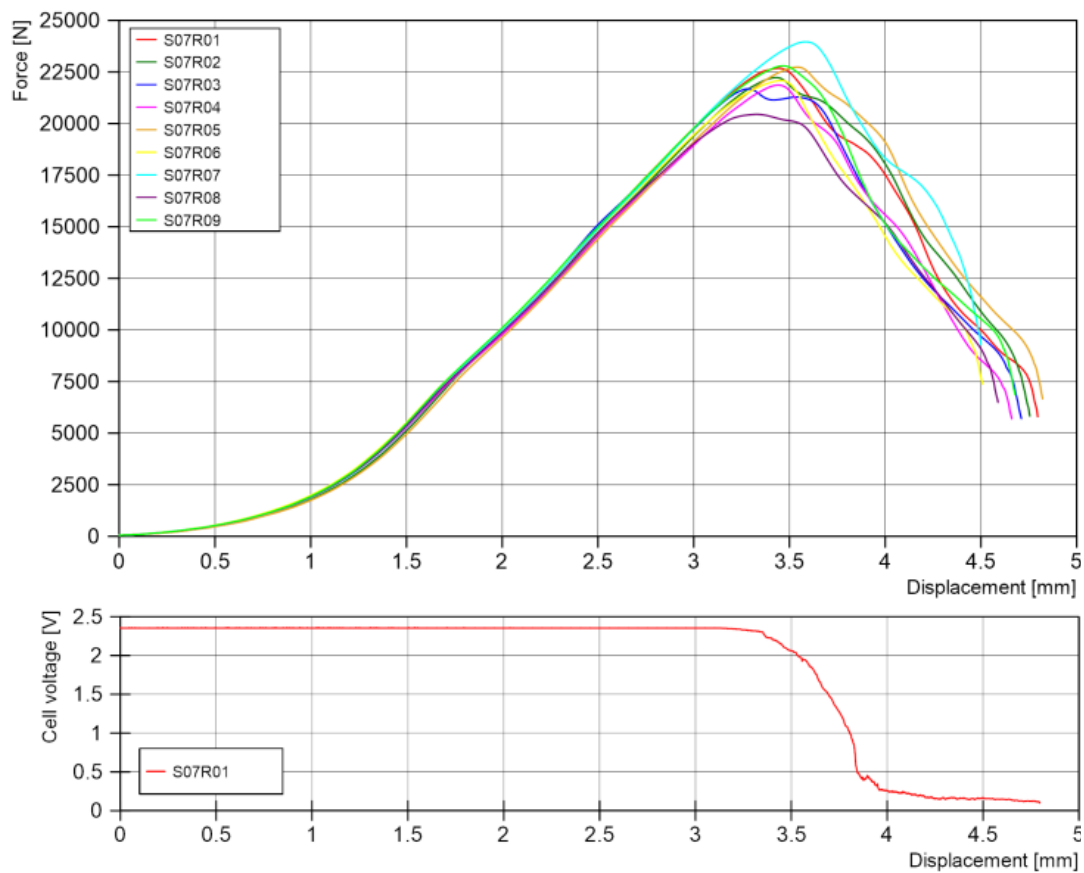


Figure 45 - Load displacement curves of a pouch cell under hemispherical head indentation for nine different position (top) and Cell voltage displacement curve (bottom)

As can be seen in Figure 45, somewhere after 3.5 mm both the Force and the Cell Voltage drop quickly, pointing out that an ISC was happening. In fact, when the displacement finally reached 4 mm, the voltage of the battery is near the 0V.

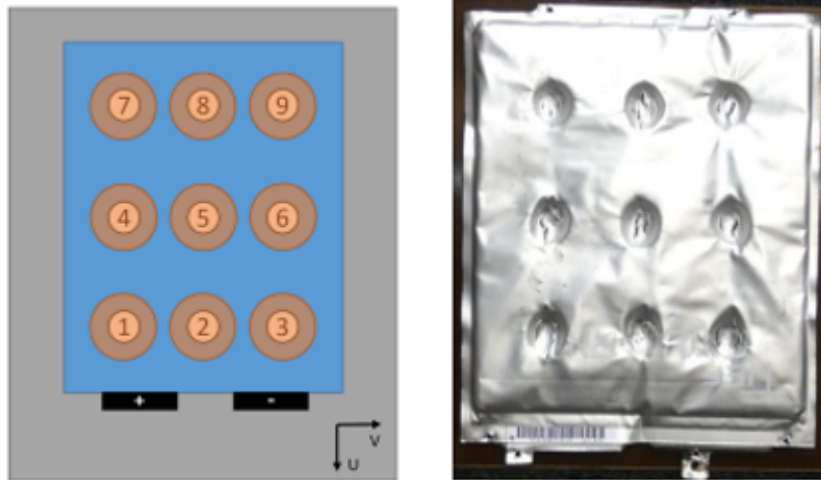


Figure 46 - Different contact points utilized during a previous test in VSI

In light of the above, the choice made was to fix the maximum value of deepness to 3mm and to use (like the previous test) a tip created by a sphere with radius equal to 15mm to accomplish the denting, being sure that the worst case scenario could be only a soft short circuit.

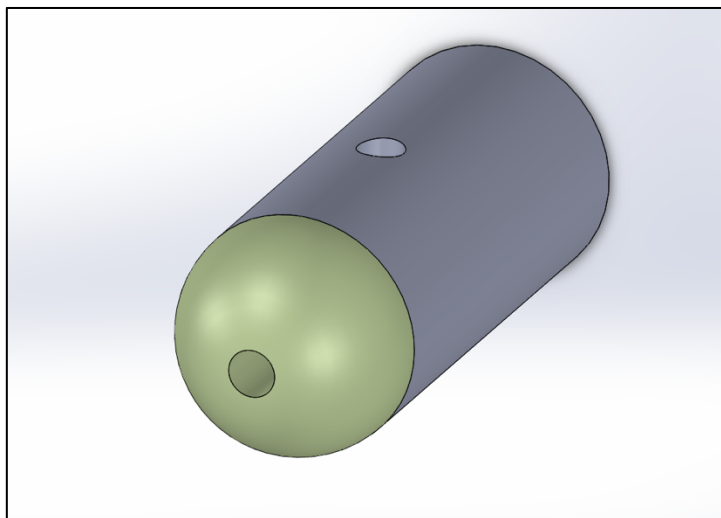
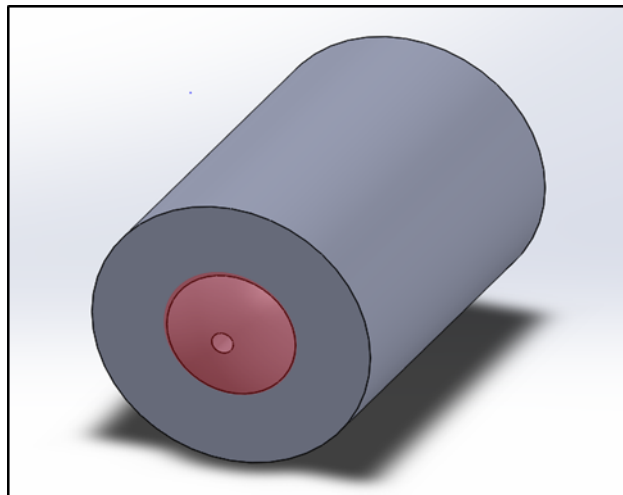


Figure 47 - First prototype of the impactor

The first prototype created in SolidWorks, as shown in Figure 47, was designed in metallic material but with the head covered in insulating material, in order to grant electrical insulation during the test. Then, was decided not to proceed with metal at all for two reasons:

- Even if the head had been covered with insulating material, the metallic body do not meet the safety standard of the test.
- Metals like iron or full metal, possible employable metals for the body, have a high coefficient of thermal conductivity. This means that if a temperature sensor wanted to be put inside the impactor to check the temperature in the site of the impact, the metal impactor could steal part of the heat coming from the battery during the test.

For these reasons, it was decided to opt for an impactor entirely made of plastic material, as can be seen in Figure 48.



*Figure 48 - Final prototype of the impactor*

A decision had to be taken between the area surrounding the tip; one way to proceed was let the tip be the entire head like in the first prototype while another way was creating a cylindrical body with a diameter bigger than the diameter of the tip ( $>18\text{mm}$ ). The difference here was how conservative the experiment had to be: with the first prototype, the layers were bent only in the longitudinal direction of the head while they were free to move in other directions. On the other hand, using the final prototype the layers were compressed not only by the head of the impactor but also from its cylindrical body. The final prototype was chosen to proceed with the tests.

In order to better describe the experiment, a temperature sensor was put inside the tip of the

impactor to have, then, the exact temperature on the site of the impact. The impactor was drilled for its entire length (63mm) to create a transit for the sensor, as can be seen in Figure 49. The double diameter of the channel is due to the characteristic of the temperature sensor, so, starting from the base of the impactor, the diameter of the channel was of 10 millimetres for 53 mm of length (to accommodate the cable), then the diameter shrink to 3 millimetres for the remaining 10 mm (to accommodate the sensor).

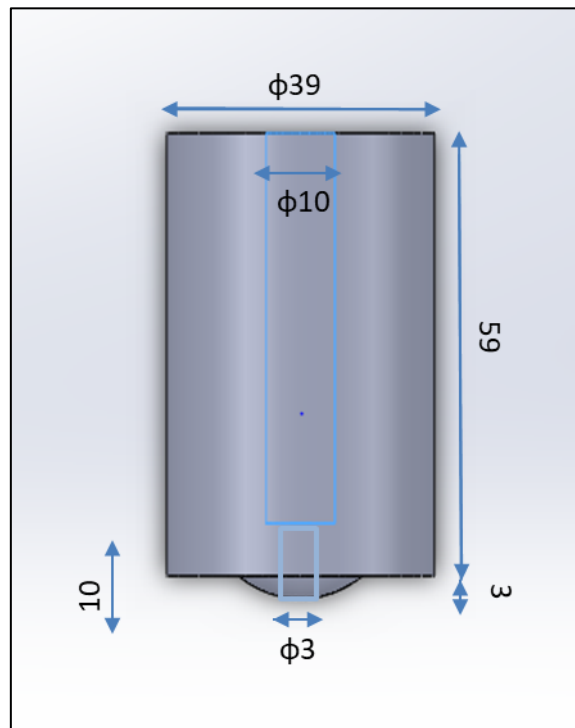


Figure 49 - Cross section of the impactor with internal channel exposed

Last, a lot of options were available regarding the position of the impact as can be seen in Figure 50. Position 1, 3 and 5 were primary taken into consideration during the design of the test; however, 1 and 3 were discontinued because even if interesting points due to nearness to edges and tabs, probably tabs that close could have a too much high influence on temperature records in the point of impact. For that reason, only the test with impact on position 5 was processed.



*Figure 50 - Explanatory image of the available point of impact*

### ***3.6 Temperature sensors***

To record in a precise way, the heat coming from the battery, eight PT1000 sensors were employed. These sensors are platinum resistance thermometer and they are an accurate method for temperature measurements. Resistance thermometers offer greater stability, accuracy and repeatability than thermocouples; the fundamental difference is that, whereas the thermocouple generates a thermoelectric voltage using the Seebeck effect to generate it, resistance thermometers are primarily a temperature-sensitive resistor that will only produce an equivalent voltage change if a constant current is passed through them, so they require a power source to operate. The resistance thermometer is based on the fact that the electrical resistance of a metal increases linearly with temperature<sup>21</sup> as shown in Figure 51 for platinum.

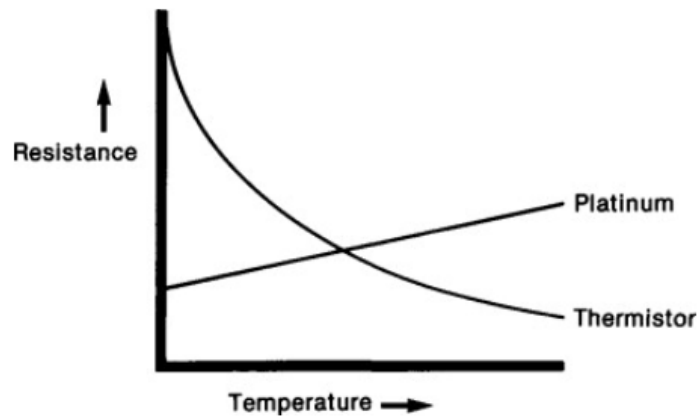


Figure 51 - Graph containing the changes of resistance with temperature for a platinum resistance thermometer and a thermistor<sup>21</sup>

Many resistance thermometers consist of a length of wire wrapped around a ceramic or glass core but other constructions are also used. The wire is a pure material, typically nickel, copper or platinum. This because these material have an accurate resistance/temperature relation which is used to provide an indication of temperature. The resistance/temperature relation is the linear approximation of the resistance versus temperature relationship between 0 and 100°C. This temperature coefficient of resistance is denoted by  $\alpha$  and has units of  $\Omega/(\Omega^{\circ}\text{C})$ :

$$\alpha = \frac{R_{100} - R_0}{100^{\circ}\text{C} * R_0} \quad (9)$$

where  $R_0$  is the resistance of the sensor at 0°C and  $R_{100}$  is the resistance of the sensor at 100°C. Platinum for example, used in this case, has the most stable resistance-temperature relationship over the largest temperature range with  $\alpha$  equal to  $0.003925 \Omega/(\Omega^{\circ}\text{C})$  and a measurement range of -200°C to 800°C.

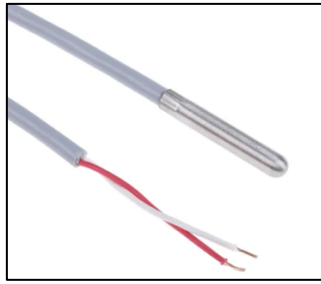


Figure 52 - PT1000 sensor

The sensors were placed in a way to best describe the thermal behaviour on battery. As can be seen from Figure 53, two sensors were positioned on tabs.

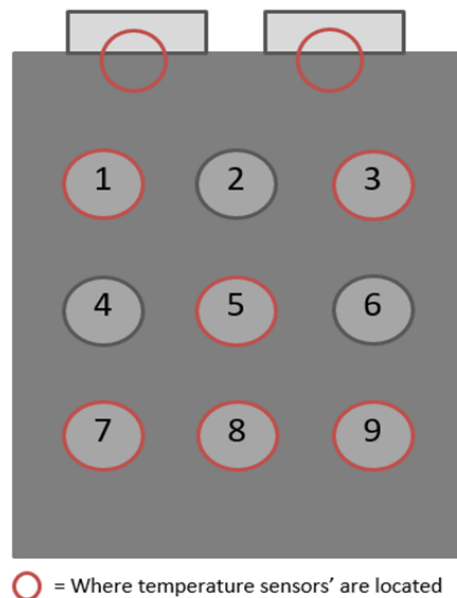


Figure 53 - Explanatory image of temperature sensors' location

This because the voltage at the terminals has been sensed by putting two crocodile cables directly in contact with the anode and cathode tabs, so that the differential voltage between them can be evaluated; this manual procedure can be tricky since the space to apply the cables was pretty limited. If a cable resulted to be badly connected, the resistance in the circuit increase, leading to an increasing of temperature. However, positioning one temperature sensor on each tab, this error then can be quickly individuated at the monitor during the test and allow to correctly position the cables. Another temperature sensor was fixed inside the impactor to record the temperature on the area of the impact while the

remaining six sensors were located circularly around the position 5 in order to investigate if some radial thermal behaviours can be noted or if some other kind of anomalies were registred.

### 3.7 Pliers and plates design

To supply the battery with energy, a connection between power supply and tabs is needed; two custom pliers were designed to grant that connection between them, as shown in Figure 54. The holes with diameter of 10mm was employed to fix the power supply cable with a M10 screw while the two holes with diameter of 6mm were used to screw together the pieces of Figure 54 and 55 and allow to grab the tabs.

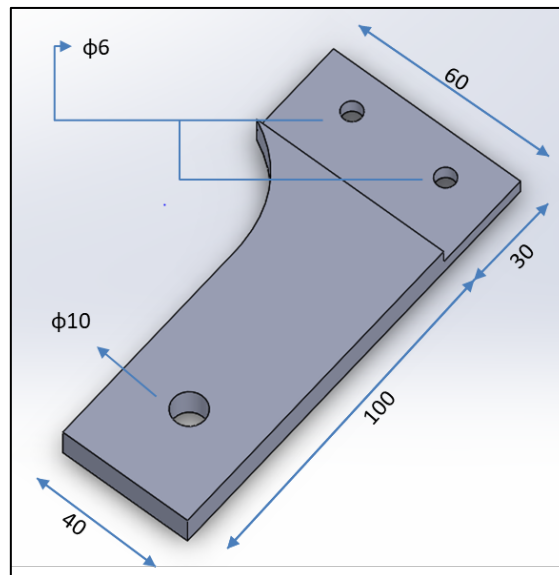


Figure 54 - Solidworks sketch of Aluminium plier

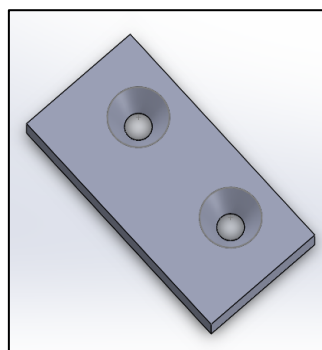
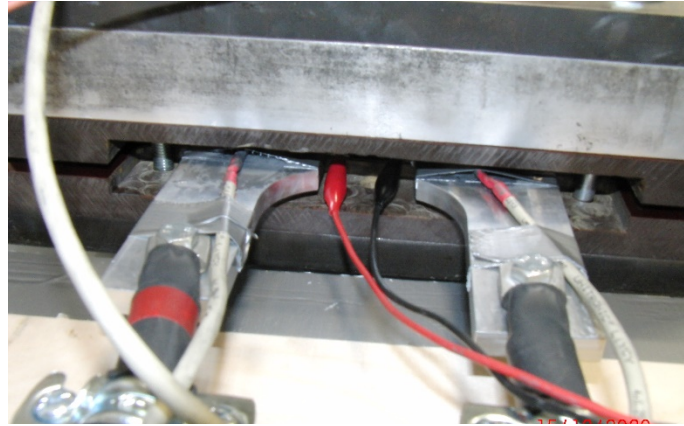


Figure 55 - Superior piece of Aluminium plier

Two PT1000 sensors were used to record the temperature on the tabs, but since it is not possible to position them directly on tabs, we fix them on the pliers using some thermal paste as shown in Figure 55.



*Figure 56 - Real Aluminium pliers under use*

The choice for the material falls for aluminium: this because a metal with high thermal coefficient was needed, in order to do not lose some heat produced on the tabs but having quickly a heat transmission.

Grant the electric insulation is necessary to accomplish the test in full safety. In order to do that, three different custom plates made of Pertinax. This material is made of hard paper which is impregnated with phenolic resin and then compressed as several layers. Pertinax in the electrical engineering industry is used as insulating material and as insulation supporting material for electronic components and printed circuit boards<sup>22</sup>. It is well-known for low specific weight and high mechanical strength and good electrical insulation properties. Two Pertinax plates were used to perform all the tests with the pristine batteries while a different plate is needed on the superior part of the sandwich when tests with the impactor were performed.

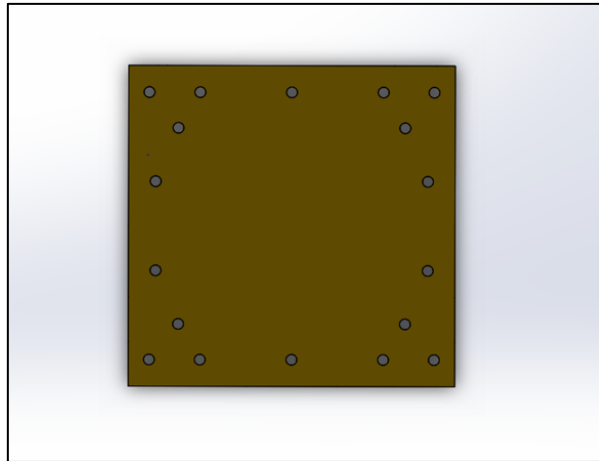


*Figure 57 - Bottom view of inferior Pertinax plate*

The manufacturer delivered on request, three plates of Pertinax 3mm thick. These required to be properly drilled to allow the transit of M12 screws, so, 18 holes 1.2mm wide were executed in the laboratory as can be seen in the SolidWorks sketch in Figure 57. In addition to this treatment, an additional socket was realized by milling, on the front of the plate as shown in Figure 58; this socket is necessary to allocate properly pliers and crocodile cables connected to the tabs.

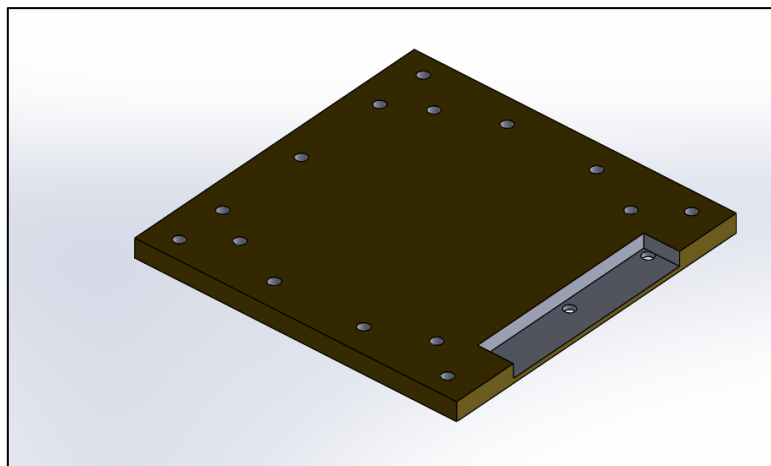


*Figure 58 - Cavalieri's axonometry of inferior plate of Pertinax*

Regarding the plate needed for the tests that employed the impactor, some modifications are needed. In the previous paragraph was described the position choice for the temperature sensors; those sensors needed to transit through the entire sandwich in order to record the

battery heat. For this reason, five holes of 0.8mm were drilled in those exact position as shown in Figure 59. In addition, a hole of 40mm was obtained by milling in allow the impactor the mechanically abuse the battery. Also in this case, the socket was obtained in the front part in a mirrored way of the inferior plate.

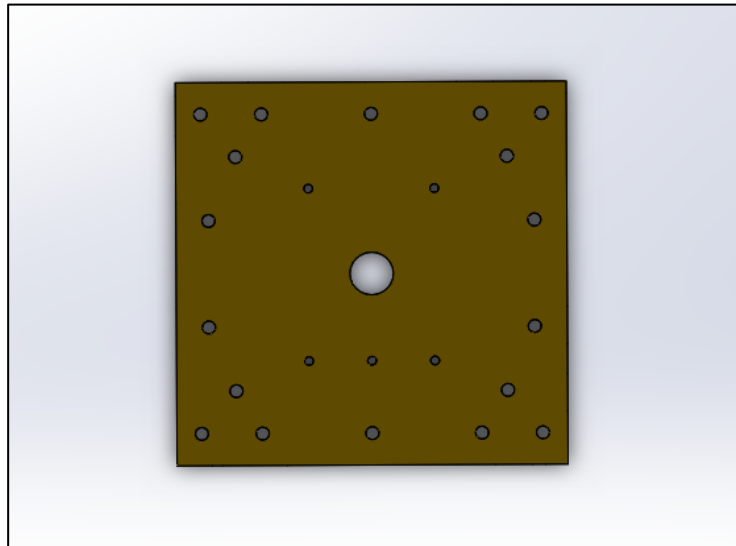


*Figure 59 - Top view of the superior Pertinax plate used to allow the transit of the impactor*

### **3.8 Mounting sequence**

For the mounting sequence, the full metal and the inferior Pertinax plate were positioned on a wood block to have then enough space to tighten the bolts as shown in Figure 59.

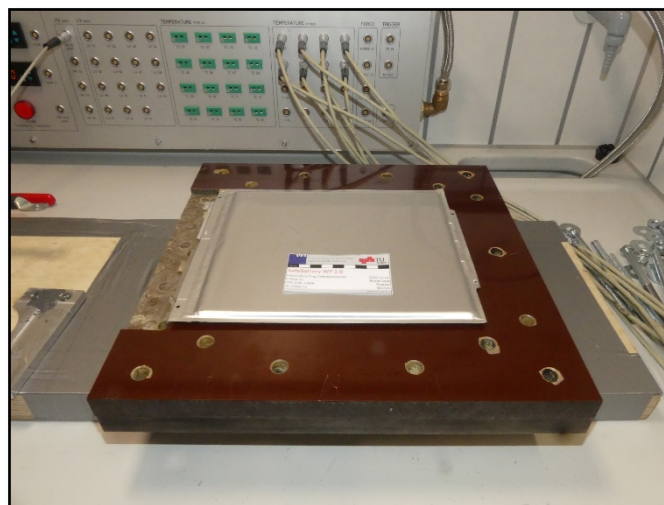


*Figure 60 - Full metal plate and Pertinax plate on wood block*

Then, the superior plate of Pertinax was add on the battery as in Figure 60.



*Figure 61 - Addition of superior Pertinax plate*

At this point, the aluminium and the full metal plates were added on the sandwich, positioning the impactor between those two plates. The inferior and superior full metal plates were then screwed together with the M12 screws.



*Figure 62 - Full sandwich for the tests*

Last, the full sandwich was positioned on the inside of a pool for safety reasons. If something during tests had gone wrong, the pool would be filled with water to interrupt immediately every kind of test.

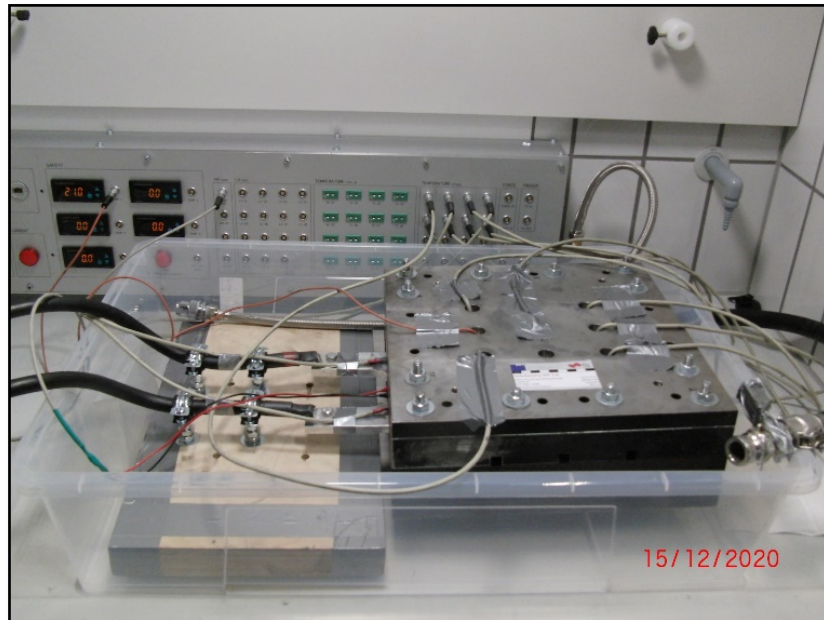


*Figure 63 - Full setup for the test*

# CHAPTER IV

## 4. Experiment results

In this Chapter the main results obtained from the tests are showed, making a comparison between the fresh battery and the mechanically loaded one. Before showing them in a precise and systematic way, a little summary of the results was included in a table to better understand what happened during the test.

### 4.1 Results of the first tested battery

The tests on the first battery proceeded without short-circuit events. In the cycling between 20% and 30% a variation in the Peak-to-Peak Voltage was detected, while in the Voltage relaxation test some variation were detected only with higher C-rate (2C and 3C).

	1C	2C	3C
Cycling 20%-30%	Detected Vpp variation	Detected Vpp variation	Detected Vpp variation
Voltage relaxation	No difference detected	Voltage relaxation variation	Voltage relaxation variation

Table 4 - Results of the first battery tested

### 4.1.1 Electrical cycling between 20% and 30% of SOC

As can be seen from Figure 64, five cycles were performed and already at 1-C rate a Peak-to-peak Voltage variation is evident.

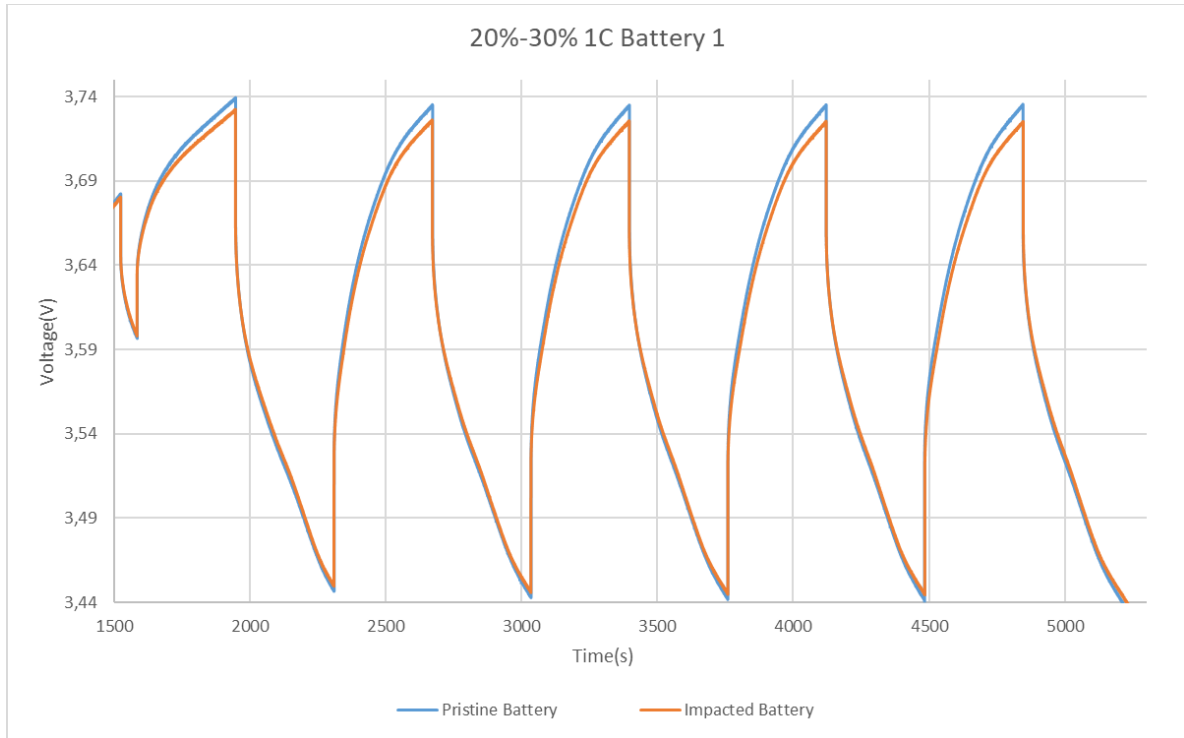


Figure 64 - Comparison between pristine battery and impacted battery in cycling between 20% and 30% of SOC at 1C-rate

In particular, considering the pristine battery, the Peak-to-peak Voltage ( $V_{pp}$ ) was calculated as:

$$V_{pp} = V_{max} - V_{min} = 3.74V - 3.54V = 0.29V$$

While for the Impacted battery:

$$V_{pp} = V_{max} - V_{min} = 3.73V - 3.45V = 0.28V$$

The difference here is less than 0.1 V. Now, it is interesting to analyse the other C-rate results in order to see if there is a C-rate dependence.

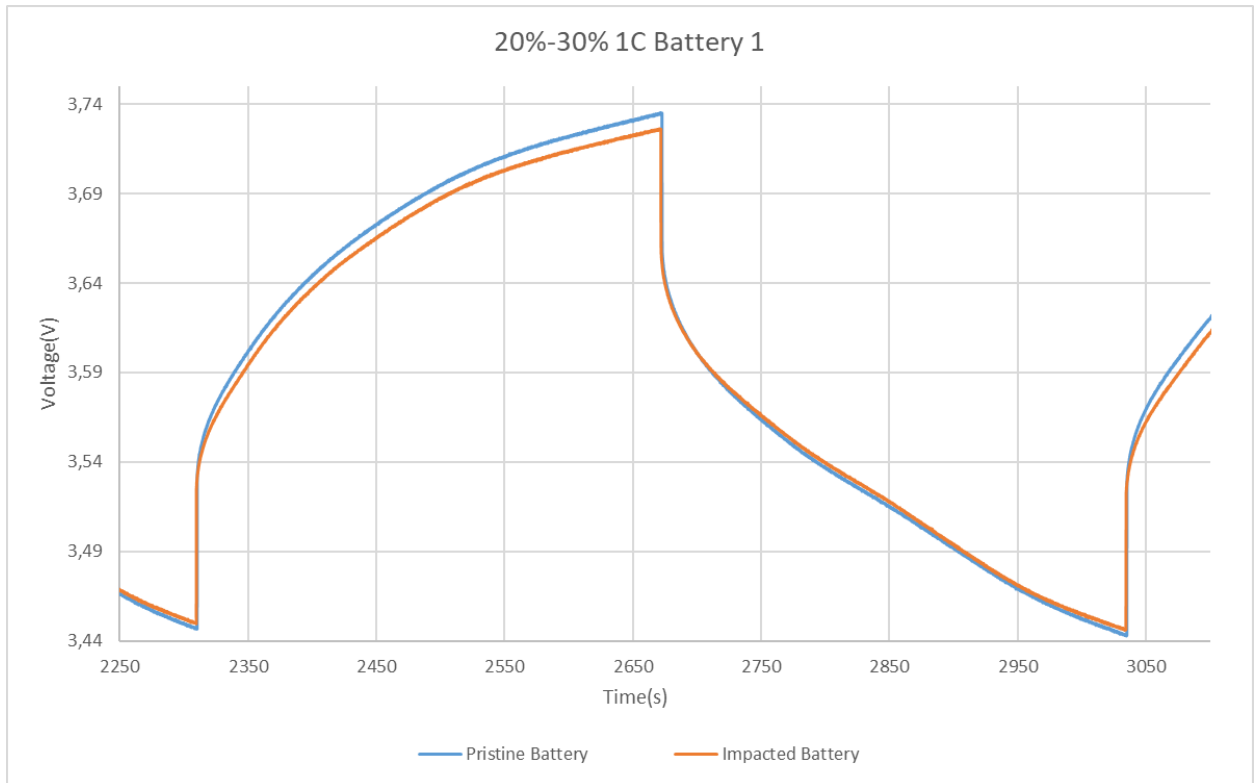


Figure 65 - Closer look to a single cycle between 20% and 30% of State of Charge at 1C-rate

For the test executed at 2C-rate, considering the pristine battery, the Peak-to-peak Voltage ( $V_{pp}$ ) was calculated as:

$$V_{pp} = V_{max} - V_{min} = 3.82V - 3.38V = 0.44V$$

While for the Impacted battery:

$$V_{pp} = V_{max} - V_{min} = 3.80V - 3.40V = 0.40V$$

The difference here is around 0.4V. It starts to get bigger as the C-rate increase.

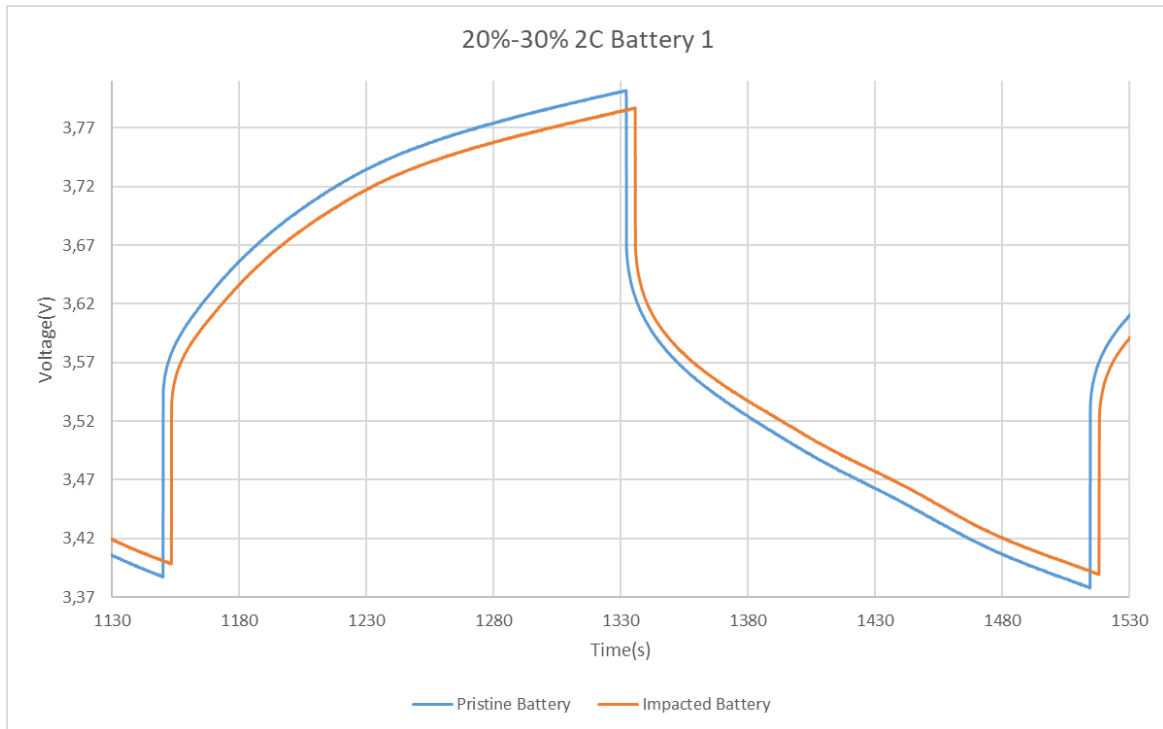


Figure 66 - Closer look to a single cycle between 20% and 30% of State of Charge at 2C-rate

Finally, as shown in Figure 67, we get the proof of some C-rate dependency because the difference of Voltage is maximum in the test at 3C-rate. Considering the pristine battery, the Peak-to-peak Voltage ( $V_{pp}$ ) was calculated as:

$$V_{pp} = V_{max} - V_{min} = 3.90V - 3.34V = 0.56V$$

While for the Impacted battery:

$$V_{pp} = V_{max} - V_{min} = 3.87V - 3.36V = 0.51V$$

The difference here is around 0.5V, still the maximum difference recorded.

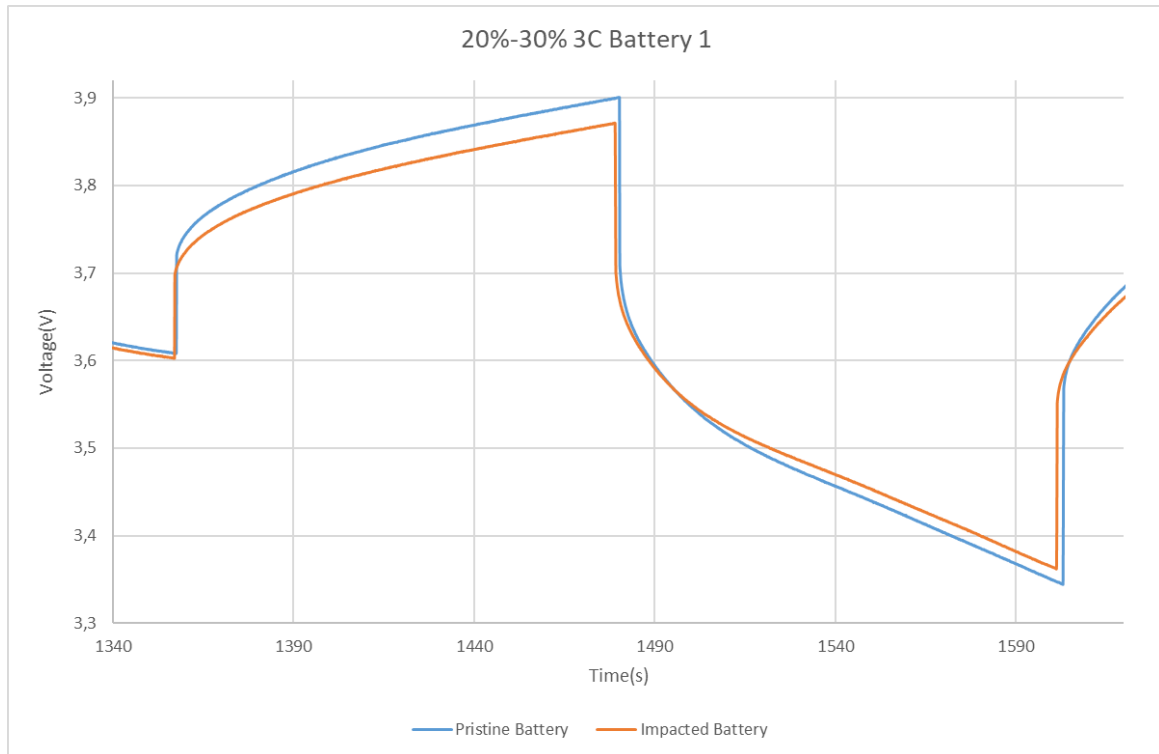


Figure 67 - Closer look to a single cycle between 20% and 30% of State of Charge at 3C-rate

#### 4.1.2 Voltage relaxation after reaching SOC of 90%

During the tests of voltage relaxation, phenomena of voltage plateau were researched but, as shown in Figure 69, 1C-rate is not sufficient to generate an, at least minimal, voltage plateau neither in the pristine battery nor in the impacted one. The difference in voltage that can be seen during relaxation between pristine and impacted battery (around 0.1V) was due to a minimal difference in the starting point at 0% SOC, as can be noted in Figure 68.

On the contrary, in the test performed at 2C-rate on the pristine battery, a consistent Voltage plateau is visible and can also be noted that after the impact, the remaining Voltage plateau seems to be reduced. Last, in the test performed at 3C-rate, the Voltage plateau in the pristine battery is the most evident between the ones obtained. Also, in this case, a C-rate dependence is demonstrated because the Voltage plateau appears reduced; on the other hand, while in the 2C-rate test the Voltage plateau seems to be totally reduced, in the 3C-rate test, a first part of plateau remains almost identical between pristine and impacted battery.

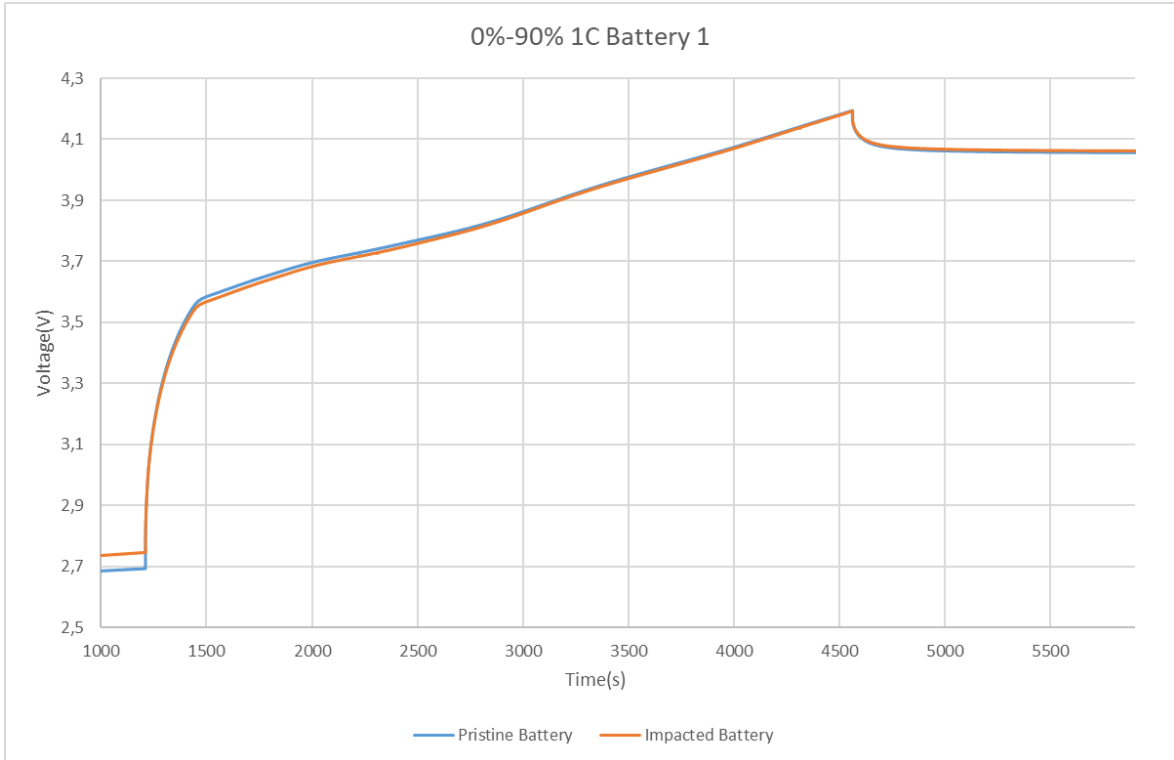


Figure 68 - Overview of charging until 90% SOC at 1C-rate followed by voltage relaxation

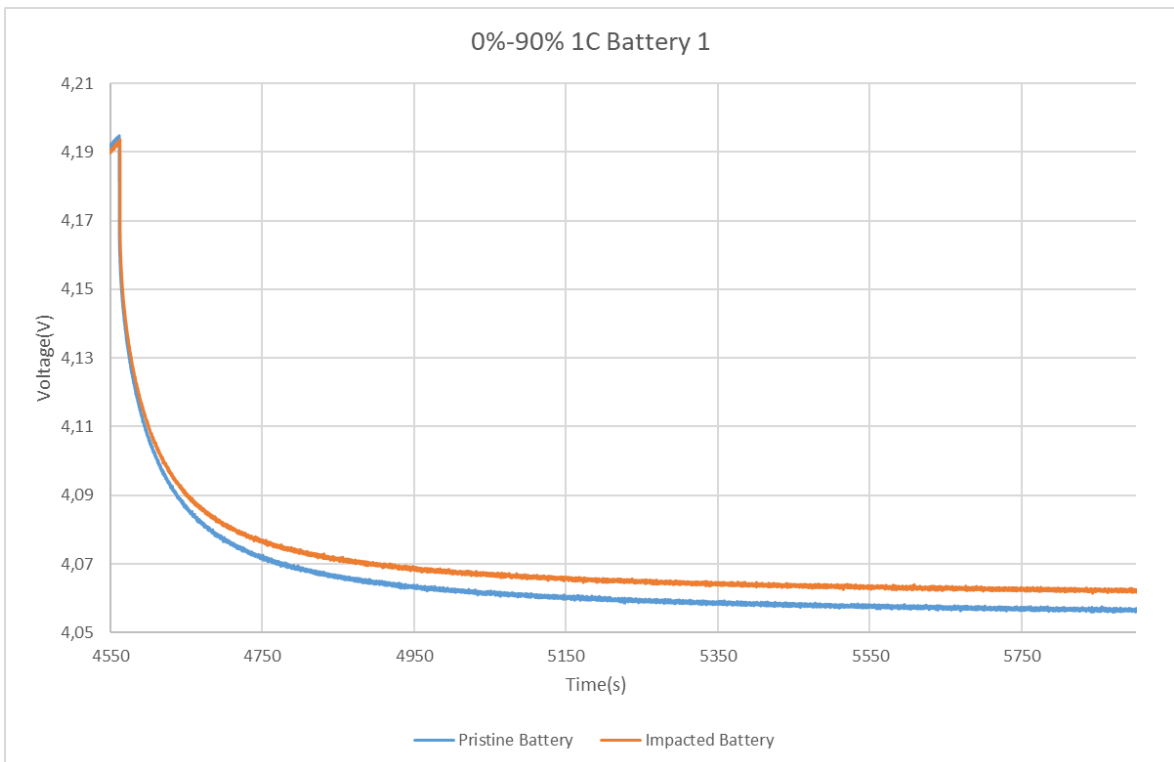


Figure 69 - Closer look to voltage relaxation executed at 1C-rate

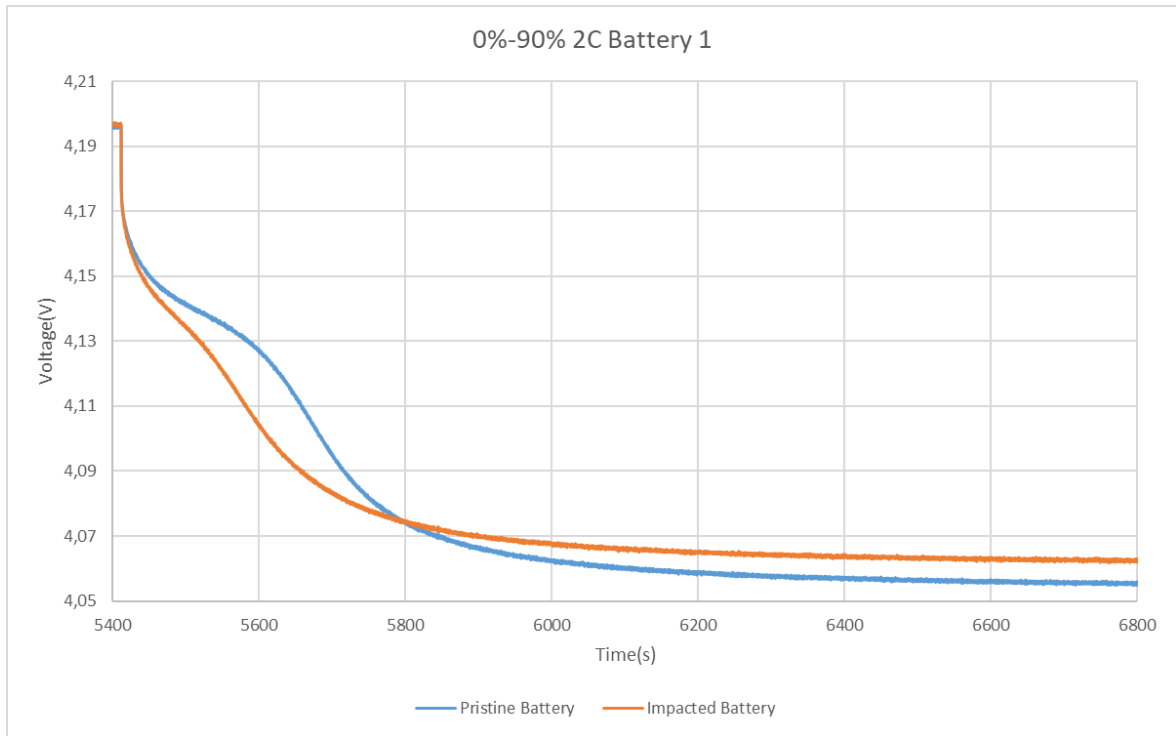


Figure 70 - Closer look to voltage relaxation executed at 2C-rate

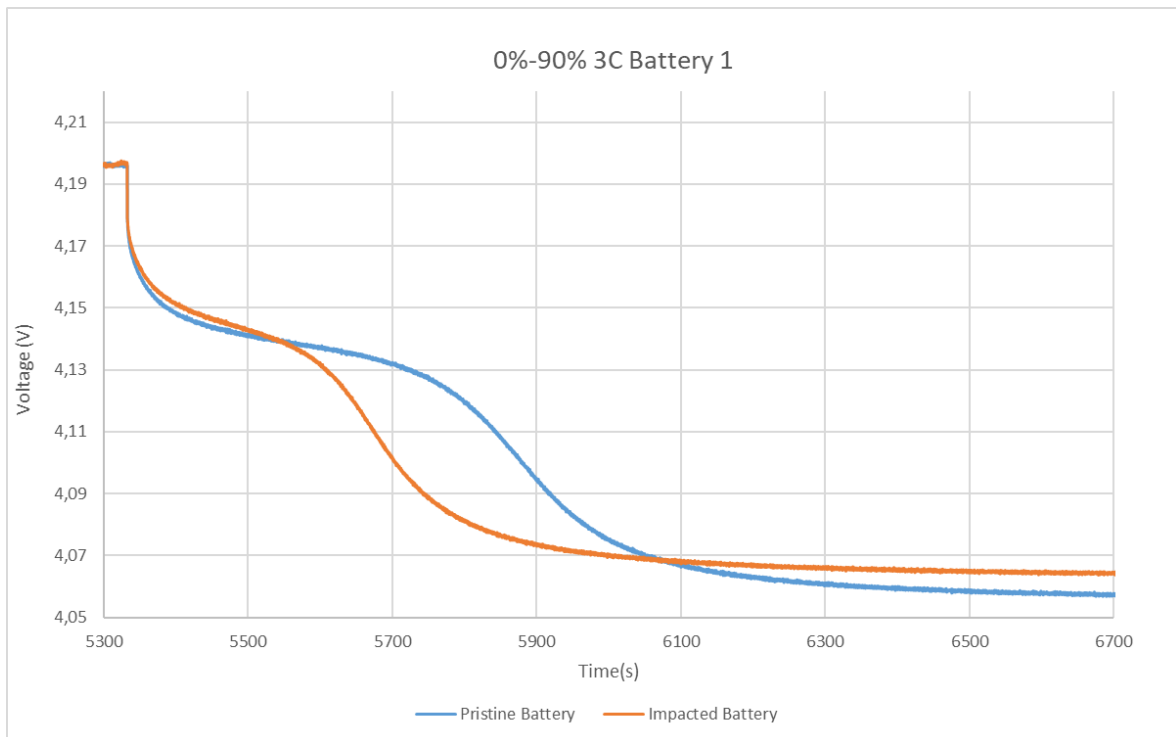


Figure 71 - Closer look to voltage relaxation executed at 3C-rate

#### 4.2 Results of the second tested battery

Both the tests on the second battery proceed without any short circuit event and, as can be seen from Table 5, in the cycling between 20% and 30% a variation in the Peak-to-Peak Voltage was detected, while in the Voltage relaxation test some variation were detected only with higher C-rate (2C and 3C).

	1C	2C	3C
Cycling 20%-30%	Detected Vpp variation	Detected Vpp variation	Detected Vpp variation
Voltage relaxation	No difference detected	Voltage relaxation variation	Voltage relaxation variation

Table 5 - Results of the second battery tested

These results are particularly important to grant the repeatability of the test; having a Voltage variation in the 20%-30% cycling and a reduction of the Voltage plateau also in the second battery gives the proof that these results can be replicated and they are not dependent from a particular manufacture of the first battery.

In particular, considering the pristine battery, the Peak-to-peak Voltage ( $V_{pp}$ ) was calculated as:

$$V_{pp} = V_{max} - V_{min} = 3.74V - 3.54V = 0.29V$$

While for the Impacted battery:

$$V_{pp} = V_{max} - V_{min} = 3.73V - 3.45V = 0.28V$$

The difference here is less than 0.1 V. Now, it is interesting to show the other C-rate results

to confirm also in this case a C-rate dependence.

For the test executed at 2C-rate, considering the pristine battery, the Peak-to-peak Voltage ( $V_{pp}$ ) was calculated as:

$$V_{pp} = V_{max} - V_{min} = 3.81V - 3.38V = 0.43V$$

While for the Impacted battery:

$$V_{pp} = V_{max} - V_{min} = 3.79V - 3.39V = 0.40V$$

The difference here is around 0.3V. It starts to get bigger as the C-rate increase.

We get the final proof of some C-rate dependency because the difference of Voltage is maximum in the test at 3C-rate. Considering the pristine battery, the Peak-to-peak Voltage ( $V_{pp}$ ) was calculated as:

$$V_{pp} = V_{max} - V_{min} = 3.86V - 3.34V = 0.52V$$

While for the Impacted battery:

$$V_{pp} = V_{max} - V_{min} = 3.83V - 3.35V = 0.48V$$

The difference here is around 0.4V, still the maximum difference recorded.

### 4.3 Results of the third tested battery

As shown from the Table 6, the tests of electrical cycling between 20% and 30% of State of Charge proceeded well for the third battery subject to test and also in this case some difference in the Peak-to-Peak Voltage were found.

	1C	2C	3C
Cycling 20%-30%	Detected Vpp variation	Detected Vpp variation	Detected Vpp variation
Voltage relaxation	Soft short circuit	X	X

Table 6 - Results of the first battery tested

For what concerns the second series of tests, the voltage relaxation ones, a soft short circuit was encountered making the successive tests with different C-rate impossible to be done. While the test from 0% to 90% at 1C-rate was in execution, during the range of time reserved to relaxation, an anomalous temperature was registered in the impacted battery. In particular, on Position 5, the one where the impact happened, some peak of temperature around 35°C were registered. The test was continued, since an increase in temperature in the range of 10-15°C is not a sure indication of Internal Short Circuit. After 500s however, the increase continued, leaving no doubts that an Internal Short Circuit, although small and extremely localized, was happening. Given the situation, for safety requirements of the laboratory, the test was interrupted to avoid strong thermal reaction of the battery. Regarding the possible origin of the Internal Short Circuit, without an in-situ analysis of the different layers with a microscope, cannot be told if it was due to some manufacturing defects of this specific battery or if the borderline situation where we put the battery was the cause of it. Since the data coming from Voltage Relaxation at 1C-rate was not complete, no voltage plateau was observable and no comparison with the pristine case was possible.

The tests on the third battery, judging the whole series of test, can be seen as a further confirmation of the previous results obtained in the cycles from 20% to 30% and as a null result regarding the test from 0% to 90% State of Charge.

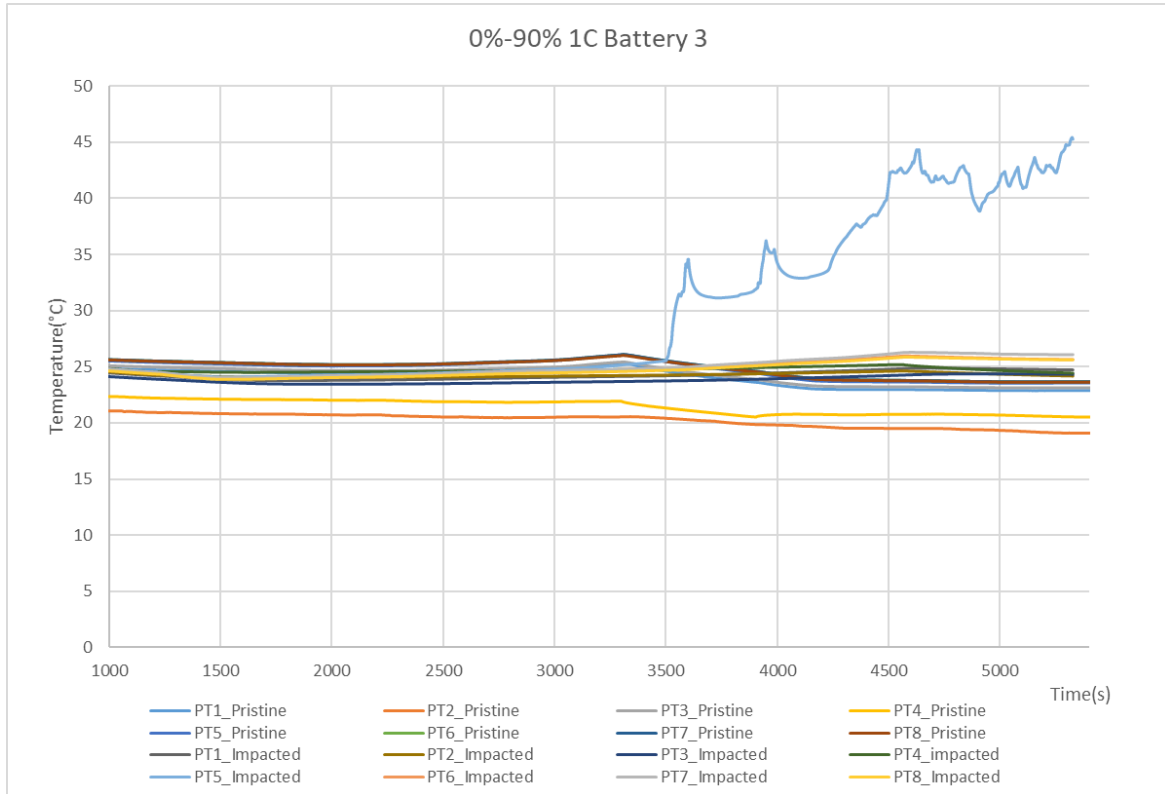


Figure 72 - Temperature data of 0%-90% 1C of third battery

# CHAPTER V

## 5. Conclusions

In this Chapter, the data coming from test were post-processed to underline the general trend that can be observe from the tests and then an explanation on the reasons behind those behaviours is provided.

### 5.1 Post-processing of data

A first data processing is done in order to find a way to quantify the reduction of Lithium Plating observed during the tests from 0% to 90% State of Charge between the pristine and the damaged batteries. In order to do that, a reference to make the comparisons need to be chosen: the curves of Voltage relaxation at 1C of the pristine battery and the impacted one were chosen as reference since, as it is confirmed in Chapter 4, current provided at 1C-rate is not sufficient to generate Lithium plating during Voltage relaxation. The choice to use the pristine curve for all the pristine comparisons and the impacted curve for all the impacted comparisons is due to small difference in Voltage (around 0.01V) between the pristine and the impacted curve that do not make possible to use a unique reference. In this way, the comparison will be more precise and reliable.

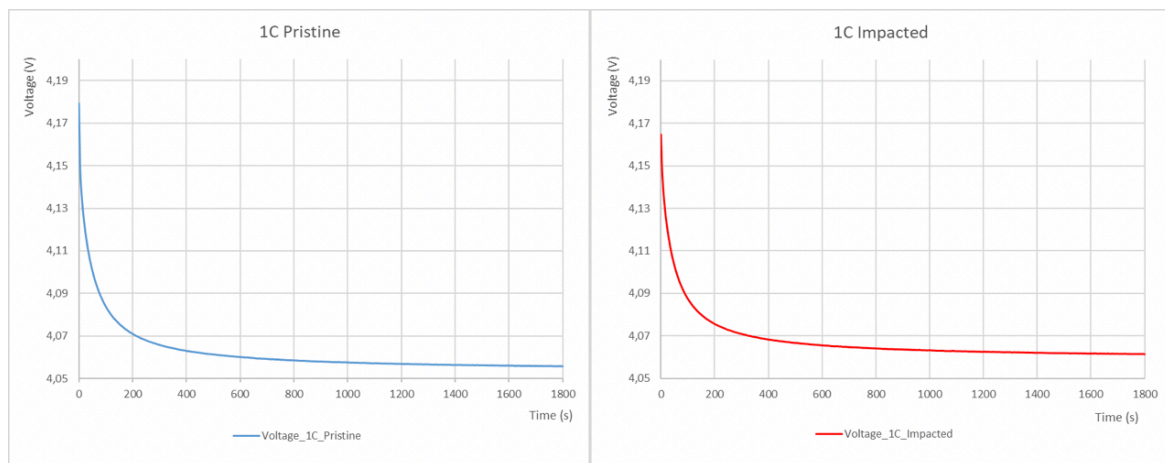


Figure 73 - Reference curves for comparisons

We need, as can be seen in the example of Figure 74, process the data to obtain a quantitative

measure of the marked region in the explicative example.

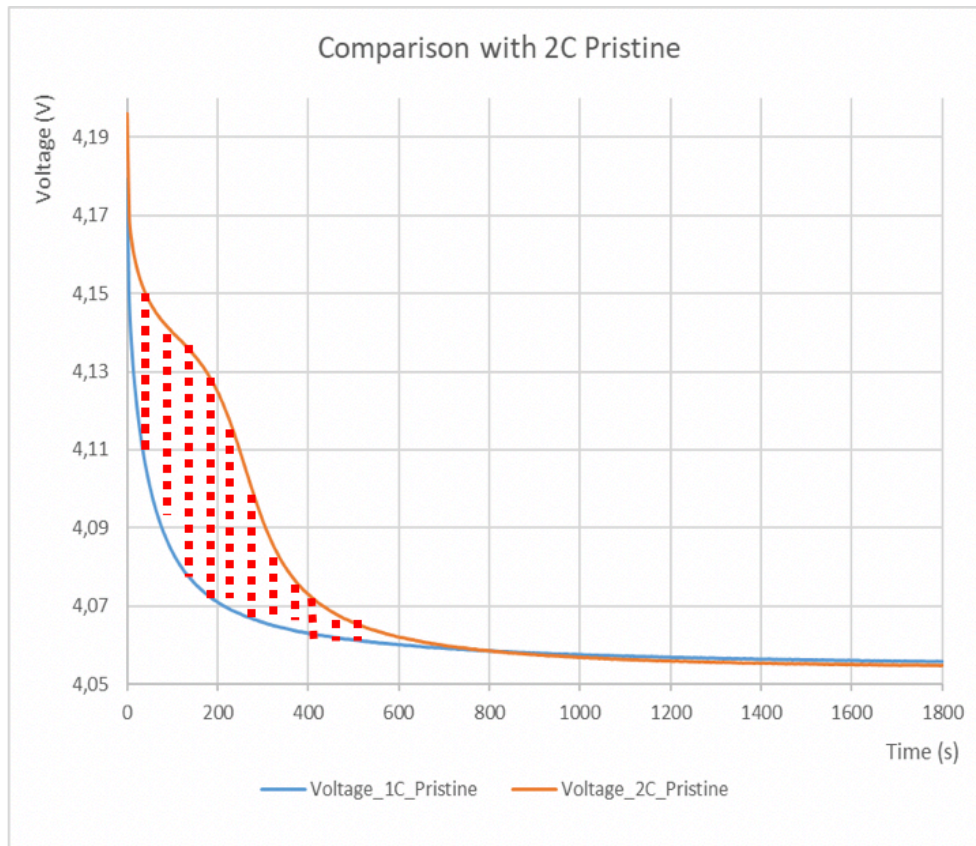


Figure 74 - Example of the type of comparison between the 1C pristine curve and 2C Pristine curve

The first step to obtain a real quantitative measure is to subtract those curves obtaining a subtracting curve. The curve that we are going to obtain are four:

$$C_1 = 2C_{\text{pristine}} - 1C_{\text{pristine}};$$

$$C_2 = 3C_{\text{pristine}} - 1C_{\text{pristine}};$$

$$C_3 = 2C_{\text{impacted}} - 1C_{\text{impacted}};$$

$$C_4 = 3C_{\text{impacted}} - 1C_{\text{impacted}}.$$

To explain the used method, only the graph to obtain the value related to  $C_1$  curve will be shown.

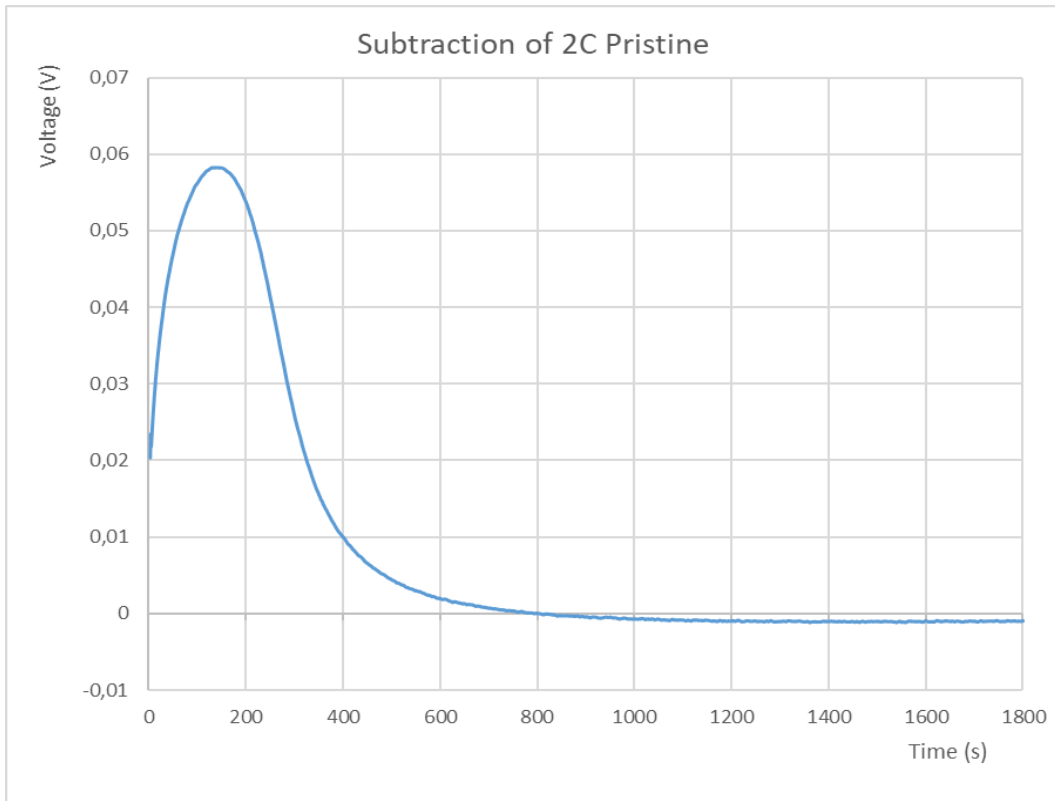


Figure 75 - Subtraction of 2C pristine curve with 1C pristine curve

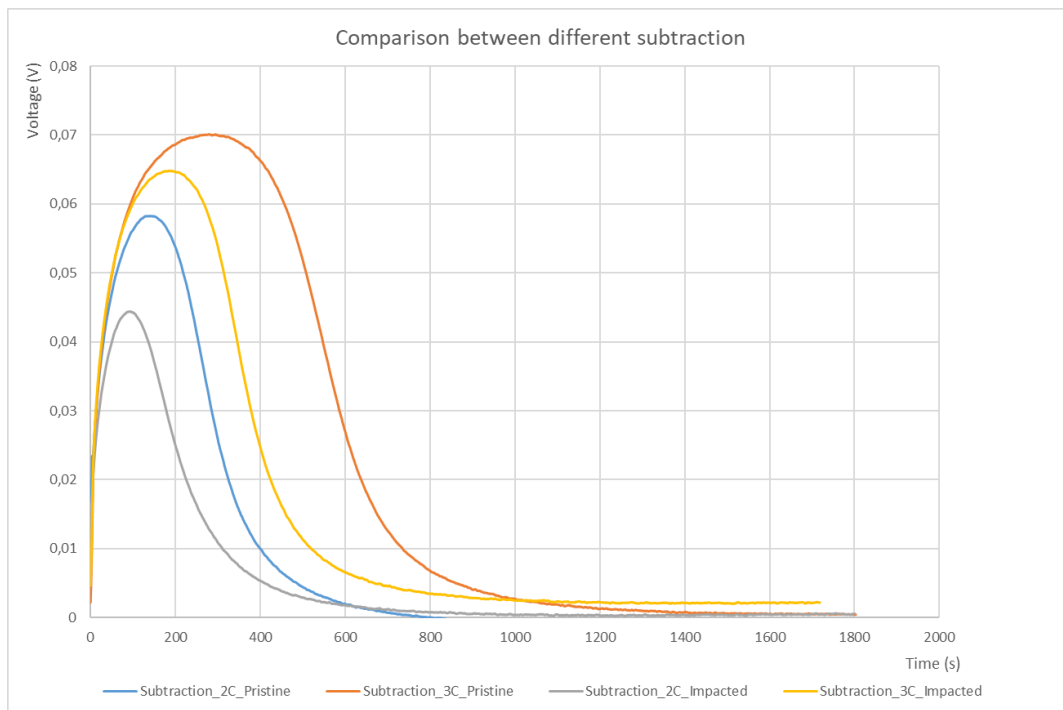


Figure 76 - Plot of all the subtraction curves obtained

The bell curves obtained give already an idea on how much Lithium plating reduces during the tests. In addition, the C-rate dependency is confirmed for sure since the higher the C-rate, the higher the reduction of Lithium plating. Once obtained all the subtraction curves, those need to be integrated in time to finally obtain the quantitative measure. Taking, for example, the subtraction curve in Figure 75, it is sufficient to stop the integration when the subtraction curve stabilizes around the zero (in this case, 800s) obtaining the curve shown in Figure 77.

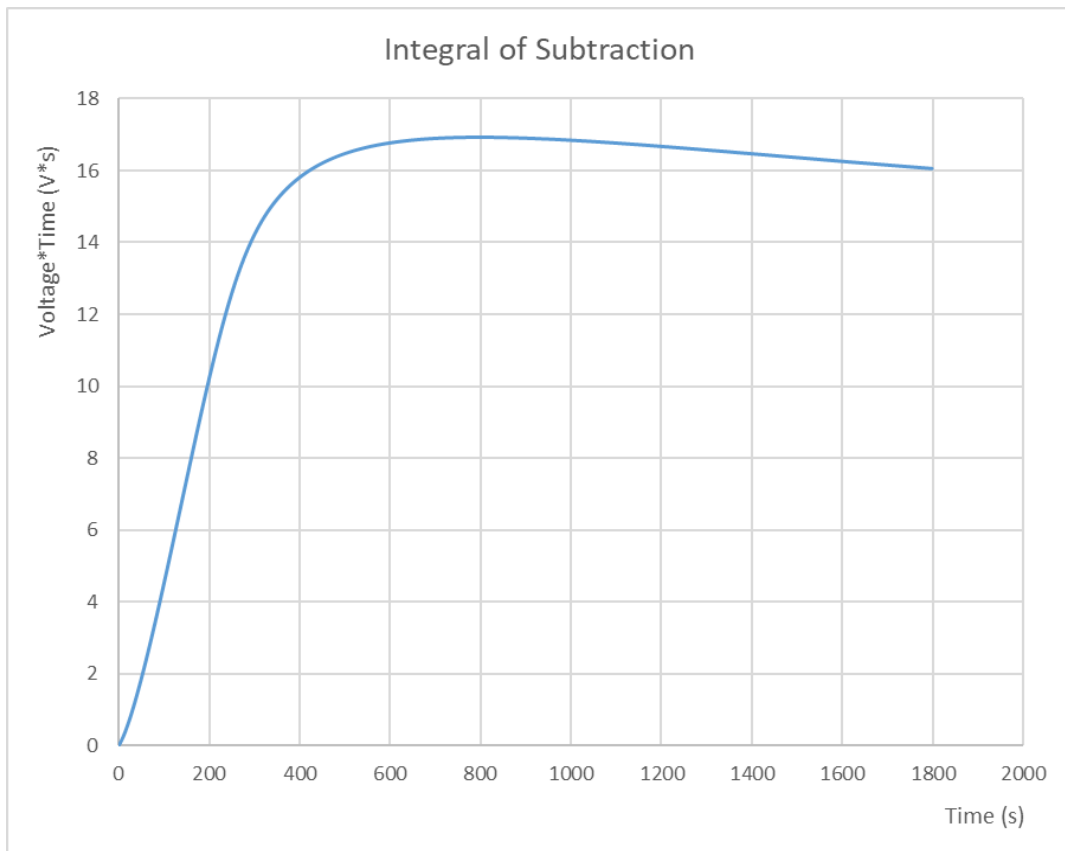


Figure 77 - Integrated curve of the subtraction

In the following Table, all the results of the integration obtained with the method just shown are included. Obviously, also from those results the reduction of Lithium plating in the impacted case is confirmed, showing also how the reduction happens at every C-rate in which the plating appears.

Integral of Subtraction [V*s]	1C	2C	3C
Pristine	0	16.6	38.8
Impacted	0	10.7	24.9

Table 7 - Results of the quantitative measures of Lithium plating

Now, let's put those values on a graph for a better visualization.

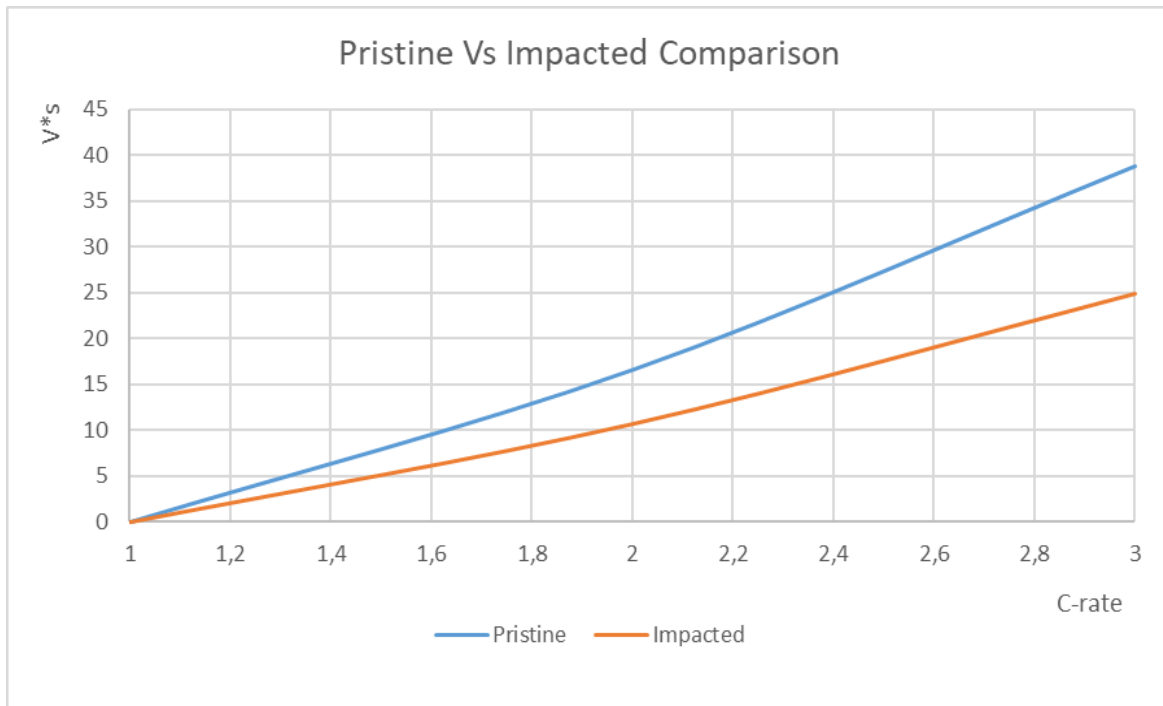


Figure 78 - Pristine versus Impacted comparison regarding Lithium plating

Even if we have only data coming from 2C and 3C, this graph can show how the reduction of Voltage plateau in the Impacted case is a trend repeatable at every C-rate. Of course, putting 0 V\*s at 1C-rate is an expedient because it would be how to say that immediately after 1C-rate Lithium plating occurs. Even if we do not have data to confirm or deny this affirmation, we can be quite sure that 1.1C or 1.2C should be not sufficient to cause Lithium plating, based on Literature notions.



## *References*

1. Elements of Physical Chemistry. Peter Atkins and Julio de Paula
2. Battery Modelling. Gregory Plett
3. N. L. Hamidah, F. M. Wang and G. Nugroho, "The understanding of solid electrolyte interface (SEI) formation and mechanism as the effect of fluoro phenylenedimaleimide (F-MI) additive on lithium-ion battery"
4. "Lithium-ion battery aging mechanisms and diagnosis method for automotive applications: Recent advances and perspectives" Rui Xiong, Yue Pan, Weixiang Shen, Hailong Li, Fengchun Sun
5. "Theory of battery ageing in a lithium-ion battery: Capacity fade, nonlinear ageing and lifetime prediction" Selcuk Atalay, Muhammad Sheikh, Alessandro Mariani, Yu merla, Ed Bower, W-Dhammika widanage
6. "Effect of current on cycle aging of lithium ion batteries" S. Barcellona, L.Piegari
7. "Understanding undesirable anode lithium plating issues in lithium-ion batteries" Qianqian Liu, Chunyu Du, Bin Shen, Pengjian Zuo, Xinqun Cheng, Yulin Ma, Geping Yin and Yunzhi Gao
8. " The understanding of solid electrolyte interface (SEI) formation and mechanism as the effect of fluoro-o-phenylenedimaleimide (F-MI) additive on lithium-ion battery" Nur Laila Hamidah, Fu Ming Wang, Gunawan Nugroho
9. "A general discussion of Li Ion Battery Safety" by Dan Doughty and E. Peter Roth
10. "Failure mechanism of Li-ion battery at overcharge conditions" D.Belov and Mo-Hua Yang
11. "Internal configuration of prismatic lithium-ion cells at the onset of mechanically induced short circuit" Hsin Wang, Simunovic, Hossien Maleki, Jason Howard, Jerald Hallmark
12. "The role of mechanically induced separator creep in lithium-ion battery capacity fade" Christina Peabody, Craig B. Arnold
13. "Road transport and CO2 emissions: What are the challenges?" Georgina Santos
14. "Lithium plating behaviour in Lithium-ion Cells" B.V.Ratnakumar and M.C. Smart
15. " Thermal runaway mechanism of lithium ion battery for electric vehicles: A review" Xuning Feng

16. "Reliability, repeatability and reproducibility: analysis of measurement errors in continuous variables" J.W.Barlett, C.Frost
17. "Fast characterization method for modelling battery relaxation voltage" An Li, Serge Pelissier, Pascal Venet, Philippe Gyan
18. "Comparative study of mechanical-electrical-thermal responses of pouch, cylindrical, and prismatic lithium-ion cells under mechanical abuse" Li Wei, Xia Yong, Chen GuanHua, Sahraei Elham
19. "Characterizing and modelling mechanical properties and onset of short circuit for three types of lithium-ion pouch cells" Elham Sahraei, Joseph Meier, Tomasz Wierzbicki
20. "Industrial ventilation design Guidebook" Pages 1105-1195 Kai Siren, Gunnar Rosen, Janos Vad, Peter Nielsen
21. "Basic Physic and measurement in anaesthesia" P.D. Davis, G.D. Parbrook and G.N.C.Kenny
22. "Pertinax- traditional material with new future" Muller Ahlorn,
23. "What is the function of the separator?" Battery University
24. "Tortuosity determination of battery electrodes and separators by impedance spectroscopy" Johannes Landesfeind, Johannes Hattendorff, Andreas Ehrl, Wolfgang Wall, Hubert Gasteiger
25. "A cell Level Model for battery Simulation" Suguna Thanagasundram, Raghavendra Arunachala, Kamyar Makinejad, Tanja Teutsch, Andreas Jossen
26. "Electrochemical methods: fundamentals and applications" Allen J. Bard, Larry R. Faulkner